UvA-DARE (Digital Academic Repository)

Alternatively spliced isoforms of TRIP8b differentially control h channel trafficking and function

Lewis, A.S.; Schwartz, E.; Chan, C.S.; Noam, Y.; Shin, M.; Wadman, W.J.; Surmeier, D.J.; Baram, T.Z.; Macdonald, R.L.; Chetkovich, D.M.

[Link to publication](#)

Cellular/Molecular

Alternatively Spliced Isoforms of TRIP8b Differentially Control h Channel Trafficking and Function

Alan S. Lewis,[1] **Emily Schwartz,**[1] **C. Savio Chan,**[2] **Yoav Noam,**[3,4,5] **Minyoung Shin,**[1] **Wytse J. Wadman,**[5] **D. James Surmeier,**[2] **Tallie Z. Baram,**[3,4] **Robert L. Macdonald,**[6,7,8] **and Dane M. Chetkovich**[1,2]

[1]The Ken & Ruth Davee Department of Neurology and Clinical Neurosciences and [2]Department of Physiology, Feinberg School of Medicine, Northwestern University, Chicago, Illinois 60611, Departments of [3]Anatomy & Neurobiology, and [4]Pediatrics, University of California, Irvine, Irvine, California 92697-4475, [5]Swammerdam Institute for Life Sciences, Center for NeuroScience, University of Amsterdam, 1098 SM Amsterdam, The Netherlands, and Departments of [6]Neurology, [7]Pharmacology, and [8]Molecular Physiology and Biophysics, Vanderbilt University Medical Center, Nashville, Tennessee 37212

Hyperpolarization-activated cyclic nucleotide-gated (HCN) channels (h channels) are the molecular basis for the current, I_h, which contributes crucially to intrinsic neuronal excitability. The subcellular localization and biophysical properties of h channels govern their function, but the mechanisms controlling these characteristics, and especially the potential role of auxiliary subunits or other binding proteins, remain unclear. We focused on TRIP8b, an h channel-interacting protein that colocalizes with HCN1 in cortical and hippocampal pyramidal neuron dendrites, and found that it exists in multiple alternative splice variants with distinct effects on h channel trafficking and function. The developmentally regulated splice variants of TRIP8b all shared dual, C terminus-located interaction sites with HCN1. When coexpressed with HCN1 in heterologous cells individual TRIP8b isoforms similarly modulated gating of I_h, causing a hyperpolarizing shift in voltage dependence of channel activation, but differentially upregulated or downregulated I_h current density and HCN1 surface expression. In hippocampal neurons, coexpression of TRIP8b isoforms with HCN1 produced isoform-specific changes of HCN1 localization. Interestingly, the TRIP8b isoforms most abundant in the brain are those predicted to enhance h channel surface expression. Indeed, shRNA knockdown of TRIP8b in hippocampal neurons significantly reduced native I_h. Thus, although TRIP8b exists in multiple splice isoforms, our data suggest that the predominant role of this protein in brain is to promote h channel surface expression and enhance I_h. Because I_h expression is altered in models of several diseases, including temporal lobe epilepsy, TRIP8b may play a role in both normal neuronal function and in aberrant neuronal excitability associated with neurological disease.

Introduction

Intrinsic neuronal excitability helps determine whether a neuron will fire an action potential in response to synaptic inputs, and thus is an important regulator of a neuron's input-output properties. Changes in expression levels and functional properties of voltage-gated ion channels regulate homeostatic activity-dependent changes in intrinsic neuronal excitability (for review, see Beck and Yaari, 2008), and may underlie abnormal excitability seen in brain disorders such as epilepsy. One type of ion channel important for determining intrinsic neuronal properties in the brain is the hyperpolarization-activated cyclic nucleotide-gated (HCN) channel (h channel), which mediates the hyperpolarization-activated current, I_h. Upregulation or downregulation of h channels and I_h controls homeostatic changes in intrinsic excitability in long-term depression (LTD) and long-term potentiation (LTP), respectively (Fan et al., 2005; Brager and Johnston, 2007), and promotes changes in cellular excitability observed in animal models of generalized absence epilepsy (Ludwig et al., 2003; Ying et al., 2007), childhood febrile seizures (K. Chen et al., 2001; Brewster et al., 2002), and temporal lobe epilepsy (Shah et al., 2004; Jung et al., 2007; Shin et al., 2008). Thus, understanding h channel regulation should shed light on mechanisms that normally control intrinsic neuronal excitability, as well as those that lead to aberrant cellular excitability in disease.

Interaction with chaperone or scaffolding molecules often determines ion channel subcellular localization and function in neurons (Lai and Jan, 2006). h channel subunits bind to and colocalize with the tetratricopeptide-repeat containing Rab8b interacting protein (TRIP8b) in distal dendrites of hippocampal and cortical pyramidal neurons (Santoro et al., 2004). Because h channels (Magee, 1998; Williams and Stuart, 2000; Lőrincz et al., 2002) are dramatically enriched in distal dendrites of hippocampal and cortical pyramidal neurons, we reasoned that TRIP8b might promote surface expression of h channels in these structures.

We studied the relationship between TRIP8b and h channels, aiming to understand the role of this protein in regulating I_h and thus intrinsic neuronal excitability. We found that alternative splicing produces multiple isoforms of TRIP8b with diverse effects on h channel surface expression and function. All TRIP8b isoforms caused a hyperpolarizing shift in voltage dependence of h channel activation, but individual isoforms differentially downregulated or upregulated I_h current density and HCN1 surface expression, implicating TRIP8b alternative splicing in the bidirectional control of h channel trafficking. Expression of distinct TRIP8b isoforms with HCN1 in neurons differentially affected HCN1 localization, consistent with a role for TRIP8b alternative splicing in h channel trafficking. We identified the two most abundant TRIP8b isoforms in the rat brain, and found these both upregulate I_h and HCN1 surface expression *in vitro*. Consistent with these findings, we demonstrated that shRNA knockdown of endogenous TRIP8b in hippocampal neurons reduces native I_h. Together, these data suggest that TRIP8b facilitates the surface expression of h channels in the brain, and may be an important regulator of h channel function in normal homeostasis and in pathological conditions such as epilepsy.

Materials and Methods

Reverse transcriptase-PCR

All animal experiments were performed according to protocols approved by the Northwestern University Institutional Animal Care and Use Committee. Reverse transcriptase (RT)-PCR was performed as previously described (Chung et al., 2009) using hippocampal total RNA isolated from neonatal through adult Sprague Dawley rat hippocampi, followed by reverse transcription and PCR amplification using primers designed to flank alternatively spliced exons or designed to amplify specific splice isoforms (see supplemental Table 1, available at www.jneurosci.org as supplemental material, for a list of primer sequences). Bands were separated on 2% agarose gel and submitted for DNA sequencing to determine the identity of amplicons.

DNA plasmids and constructs

General. All restriction enzymes were purchased from New England Biolabs (NEB). All oligonucleotides for use in PCR amplification and oligo insertion were synthesized by Integrated DNA Technologies. The proper introduction of all mutations and deletions was verified by DNA sequencing.

TRIP8b isoform constructs. cDNA encoding mouse TRIP8b_IsoB2 (GenBank accession number AB032591) in pEGFP-C1 (Clontech) was kindly provided by Drs. Bina Santoro and Steven Siegelbaum (Columbia University, New York, NY). Enhanced green fluorescent protein (EGFP) was removed by *Nhe*I/*Xho*I digestion followed by blunting and religation to yield untagged TRIP8b_IsoB2 in pXEGFP-C1 (pXEC-TRIP8b_IsoB2). The unique N terminus of TRIP8b_IsoA2 containing a silent *Spe*I site at the beginning of exon 5 was commercially synthesized (Genscript) and subcloned into pXEC-TRIP8b_IsoB2 at the *Eco*RI/*Bgl*II sites to generate pXEC-TRIP8b_IsoA2. pXEC-TRIP8b_IsoA4 was generated by PCR using primers written 5′-3′ [forward (For)–CGCGAATTCGCCACCATGTACCAGG-GACACATGCAGGGAAAAGGCTCTAGGG and reverse (Rev)–CGC-CGCCTCGAGCCCGGGTCAAGGATCCAAATTGAAAG (hereafter referred to as TRIP-CDE3′)] followed by subcloning into the *Eco*RI/*Bgl*II sites of pXEC-TRIP8b_IsoB2. pXEC-TRIP8b_IsoA5 was generated by *Eco*RI/*Spe*I digestion of pXEC-TRIP8b_IsoA2 followed by insertion of oligonucleotides (For–AATTCGGATCCGCCACCATGTACCAGGGACACATGC-AA and Rev–CTAGTTGCATGTGTCCCTGGTACATGGTGGCGGA-TCCG). pXEC-TRIP8b_IsoB4 was generated by PCR using primers (For–CGCGAATTCGGATCCGCCACCATGCAGATGAGCTACTTGAAAAG-TAAAGAACAAGGC and Rev–TRIP-CDE3′) followed by subcloning the PCR product into pXEC-TRIP8b_IsoB2 at *Eco*RI/*Bgl*II sites. pXEC-TRIP8b_IsoB1 was generated by two-part PCR, first by primers (For–CGC-GAATTCGCCACCATGTCTGACAGTGAAATGGATGGAAGGACTC (IsoB15′) and Rev–CTCGTCACTGCTTAGCTTGCCATAG) and (For–C-

TATGGCAAGCTAAGCAGTGACGAG and Rev–TRIPCDE3′), followed by PCR across the two fragments and subcloning of the PCR product into the *Eco*RI/*Bgl*II sites of pXEC-TRIP8b_IsoB2. pXEC-TRIP8b_IsoB3 was generated by PCR using the same primers as for IsoB4, with pXEC-TRIP8b_IsoB1 as template. Finally, pXEC-TRIP8b_ΔN-TRIP8b and pXEC-TRIP8b_IsoT were made by PCR using primers (For–CGCGAATTCGCCACCATGCTG-GTGAATGAGCAACAAGAGAGCAGAC and For–CGCGAATTCACCA-CCATGCAGGCAGAATGGGAGG, respectively, with Rev– TRIPCDE3′), and subcloned *Eco*RI/*Bgl*II and *Eco*RI/*Bam*HI respectively in pXEC-TRIP8b_IsoB2.

HCN1 constructs. Mouse HCN1 and HCN2 cDNA in pGHE and pEGFP-C1 expression vectors were kindly provided by Drs. Bina Santoro and Steven Siegelbaum (Columbia University, New York, NY) and subcloned at *Hin*dIII/*Eco*RI into expression vector pGW1. HCN1 was tagged by addition of the hemagglutinin (HA) epitope to the extracellular loop between transmembrane segments S3 and S4 in a similar location as previously used for HCN2 (Santoro et al., 2004). *Kpn*I and *Nhe*I sites were added to HCN1 by 2-part PCR, followed by HA oligo insertion at *Kpn*I/*Nhe*I sites. HCN1 was GFP-tagged at the C terminus by first subcloning HCN1 into pcDNA3 expression vector at *Hin*dIII/*Eco*RI using PCR. A *Bam*HI site was then introduced into HCN1 between HCN1 alanine residues 885 and 886 after which cDNA encoding EGFP was inserted by PCR cloning.

Yeast two-hybrid constructs. Bait and prey constructs were prepared by PCR amplification of the appropriate HCN1 and TRIP8b base pairs and subcloned into pGBKT7 or pGADT7 (Clontech), respectively.

Lentiviral constructs. Hairpin oligonucleotides were phosphorylated by T4 polynucleotide kinase (NEB) followed by annealing by incubation at 95°C for 30 s, 60°C for 10 min, and cooling to 20°C by 1°C every 15 s. The following oligonucleotides were used (all written 5′-3′): for TRIP8b-sh3, TTTGCCAGAGACATCATCCTTAGATTCAAGAGATCTAAGG-ATGATGTCTCTGGCTTTTT and CGAAAAAGCCAGAGACATCAT-CCTTAGATCTCTTGAATCTAAGGATGATGTCTCTGG; for TRIP8b-sh4, TTTGAGCATTTGAAGAAGGCTTAATTCAAGAGATTAAGCC-TTCTTCAAATGCTCTTTTT and CGAAAAAGAGCATTTGAAGAAG-GCTTAATCTCTTGAATTAAGCCTTCTTCAAATGCT; and for shControl (Bartkowska et al., 2007), TTTGTTCTCCGAACGTGT-CACGTTTCAAGAGAACGTGACACGTTCGGAGAATTTTT and CG-AAAAATTCTCCGAACGTGTCACGTTCTCTTGAAACGTGACACG-TTCGGAGAA.

Hairpin constructs were inserted into the expression vector pCMV-U6 (a kind gift from Dr. Pavel Osten, Cold Spring Harbor Laboratory, Cold Spring Harbor, NY) via *Bbs*I/*Bst*BI. As a second step, hairpin sequences together with the U6 promoter (U6-shRNA cassette) were released from pCMV-U6 vector by digestion with *Nhe*I/*Bst*BI and inserted into the lentiviral vector FUGWlinker (gift from Dr. Pavel Osten) (Dittgen et al., 2004).

Antibody generation

Antibodies specific to TRIP8b N-terminal exons [guinea pig (gp) α-Ex 1a-5, gp α-Ex 2, and gp α-Ex 4] were prepared commercially (Affinity Bioreagents) by immunizing guinea pigs with maleimide-conjugated synthetic peptides (peptide sequences, all contain a C-terminal cysteine for conjugation: Ex 1a-5: MYQGHMQLVNEQC, Ex 2: KSKEQ-GYGKLSSDEDLEIC, Ex 4: RAADKAVAMVMKEIPREEC). Antibodies were purified by affinity chromatography, and antigen-depleted IgG was collected for use as a negative control. cDNA encoding full-length green fluorescent protein was generated by PCR using primers (written 5′-3′; forward–GCGTGTACGGTGGGAG and reverse–CGCGAATTCTCAG-GATCCCTTGTACAGCTCGTCC) followed by subcloning the PCR product into the *Bam*HI site of the glutathione *S*-transferase (GST)-producing vector, pGEX-4T1 (Pharmacia). The resulting GST-GFP fusion protein was expressed in BL21 bacteria (Stratagene) and purified by glutathione-Sepharose affinity chromatography according to the manufacturer's protocol (Amersham Biosciences). Rabbits and guinea pigs were immunized (Affinity Bioreagents) with the GST-GFP fusion protein to generate immune and preimmune serum, and one rabbit and guinea pig yielded the sensitive and specific serum used in these studies (see supplemental Fig. 3, available at www.jneurosci.org as supplemental

material). gp antibodies to total TRIP8b were generated as previously described for rabbit α-TRIP8b [(Shin et al., 2008); for antibody characterization, see supplemental Figure 3, available at www.jneurosci.org as supplemental material].

Antibodies
The following primary antibodies were used: mouse (ms) monoclonal antibodies to α-tubulin (DM1A, Upstate Biotechnology); rabbit (rab) polyclonal antibodies to HCN1 (Alomone Labs); ms monoclonal to HA epitope (F-7, Santa Cruz Biotechnology); guinea pig (gp) polyclonal antibodies to HCN1 (Shin and Chetkovich, 2007); gp polyclonal antibodies to HCN2 (Shin et al., 2006); rab and gp polyclonal antibodies to green fluorescent protein (see antibody generation and supplemental Fig. 3, available at www.jneurosci.org as supplemental material); rab polyclonal antibodies to TRIP8b (Shin et al., 2008); gp polyclonal antibodies to TRIP8b (see antibody generation and supplemental Fig. 3, available at www.jneurosci.org as supplemental material); gp polyclonal antibodies to HCN4 (Shin et al., 2008); gp polyclonal antibodies to TRIP8b exon 1a-5, exon 2, and exon 4 (see antibody generation and Fig. 5); ms monoclonal to MAP-2 (Sigma).

Yeast two-hybrid assays
Directed yeast two-hybrid interaction assays were performed as previously described (Cuadra et al., 2004).

Preparation of lysates for Western blotting and coimmunoprecipitation assays
Adult Sprague Dawley rats were deeply anesthetized by isoflurane, followed by rapid decapitation and regional brain dissection. Protein extracts were generated by lysis in ice-cold RIPA buffer (150 mM NaCl, 1% NP-40, 0.5% deoxycholic acid, 0.1% SDS, and 50 mM TRIS, pH 8.0) containing protease inhibitors followed by centrifugation at $6000 \times g$ for 2 min and centrifugation of the supernatant at $16,000 \times g$ for 30 min. For overexpression studies, human embryonic kidney 293 (HEK293T) cells (ATCC) were grown in DMEM (Invitrogen) containing 10% fetal bovine serum (Invitrogen), penicillin, and streptomycin (Sigma). Cells were transfected using Lipofectamine 2000 reagent according to the manufacturer's protocol (Invitrogen). Plasmids were used to transfect HEK293T, and total cell lysates were made by sonication in ice-cold TEEN-Tx [TEEN buffer (50 mM Tris-HCl, pH 7.4, 1 mM EDTA, 1 mM EGTA and 150 mM NaCl) containing 1% Triton X-100].

Coimmunoprecipitation assays
Antibodies were added to lysates for 2 h at 4°C, then 20 μl of prewashed protein A/G beads (Thermo Scientific) were added and samples incubated for another 2 h at 4°C. Beads were precipitated and washed six times with cold TEEN-Tx then eluted in SDS-containing sample buffer and boiled for 2 min before SDS-PAGE. Surface HA immunoprecipitation was performed in a manner similar to that used by Vandenberghe et al. (2005). Briefly, transfected HEK293T cells were incubated with ms α-HA diluted 1:200 in DMEM at 37°C for 20 min. After incubation, cells were rinsed three times in warm DMEM followed by two times in ice-cold PBS, at which point cells were collected and lysed in TEEN-Tx. Protein A/G beads were used to immunoprecipitate bound ms α-HA and were washed six times with cold TEEN-Tx followed by Western blotting as described below.

Western blotting
Western blotting was performed as previously described (Shin et al., 2008). Primary antibody concentrations used were gp α-HCN1 (1:2000), rab α-HCN1 (1:500), gp α-HCN2 (1:2000), gp α-HCN4 (1:1000), rab α-TRIP8b (1:10,000), gp α-TRIP8b (1:4000), gp α-TRIP8b exon 1a-5 (1:7500), gp α-TRIP8b exon 2 (1:750), gp α-TRIP8b exon 4 (1:30,000), α-α-tubulin (1:10,000), and gp and rab α-GFP (1:2000). Densitometric quantitation of band intensity was performed using NIH ImageJ software. Statistical analysis was performed with Prism software (Graph-Pad). $p < 0.05$ was considered significant.

Primary neuronal culture and transfection for HCN1 and TRIP8b overexpression studies
Primary cultures were prepared from dissociated hippocampi of postnatal day 0 (P0) Sprague Dawley rats. Hippocampi were quickly dissected,

removed from adherent meninges, and incubated with 10 U/ml papain (Worthington) for 30 min. After removal of papain, cells were mechanically triturated and plated at density of 400–600 cells/mm^2 on 12 mm coverslips precoated with poly-D-lysine (Sigma). Cultures were maintained at 36°C, 5% CO$_2$, in Neurobasal/B-27-based medium (Invitrogen) that was preconditioned for 24 h in 1- to 2-week old non-neuronal cell culture prepared from P3–P4 rat cortices. Cultures were refreshed twice weekly with the conditioned medium. On the third day *in vitro* (DIV 3), 1 μM cytosine-arabinoside (Invitrogen) was added to the culture media to inhibit glial proliferation. Primary neuronal cultures were transfected with plasmid DNA on DIV 8–9 using Lipofectamine 2000 according to manufacturer's recommendations (Invitrogen). Briefly, a transfection mix that included 2 μl of Lipofectamine reagent and 1 μg of plasmid DNA was incubated at room temperature for 20 min, then added to the cultured neurons. One and a half hour after transfection, the culture medium was refreshed with warm Neurobasal medium plus B27 supplement (Invitrogen). All experiments were performed 24 h after transfection. A 1:1 ratio of DNA was maintained when cotransfecting two DNA constructs.

Immunocytochemistry for HCN1 and TRIP8b overexpression studies
Primary neuronal cultures were fixed with PBS plus 4% paraformaldehyde for 20 min on ice, permeabilized with PBS containing 0.1% Triton X (PBS-T), and blocked with PBS plus 10% bovine serum albumin (BSA, Sigma) for at least 1 h at room temperature. Subsequently, neurons were incubated with primary antibodies (gp α-TRIP8b, 1:4000; ms α-MAP-2, 1:16,000) in PBS plus 3% BSA overnight at 4°C. After washing, neurons were incubated in goat α-gp biotin-conjugated IgG (Vector) for 30 min, then streptavidin-Alexa 568 (1:1000; Invitrogen) for another 30 min. Images of the fixed neurons were captured using a laser-scanning confocal microscope (Olympus IX-70; Olympus), equipped with a 60× objective (numerical aperture, 1.40) using LaserSharp 2000 (Bio-Rad) acquisition software. Green fluorescent protein was visualized directly by green fluorescence. Similar acquisition and analysis settings for cells from each experiment were used. Line-profile plots were generated using NIS-elements-D software (Nikon). Intensity is presented in arbitrary units based on pixel brightness (in the range of 0–255). Final adjustments and image processing were made in Photoshop (Adobe). The original red color of TRIP8b-labeled neurons was pseudocolored blue. Experiments using imaging of transfected neurons were performed at least in duplicates (in most cases three coverslips per condition) and were repeated at least three times, showing consistent results.

Validation of shRNA efficacy in HEK293T cells
TRIP8b knockdown by shRNA constructs was assessed by cotransfection in HEK293T cells of TRIP8b IsoA4, pCMV-U6 containing the shRNA cassette to be tested, and GFP (to serve as control for transfection efficiency). A 1:5 molar ratio of TRIP8b IsoA4:pCMV-U6-shRNA was used for transfection (Tiscornia et al., 2006). After 48 h, cells were lysed and Western blotting was performed as described above. Membranes were probed with rab α-TRIP8b, gp α-GFP, and ms α-tubulin.

Preparation of lentiviruses and transduction
Lentiviruses were prepared by three plasmid transfection of expression plasmid FUGWlinker (described above) and the helper plasmids CMV-VSVg and CMVΔR8.9 (Lois et al., 2002). In two 15 cm culture plates per virus, HEK293T cells were transfected with FUGWlinker (20 μg), CMV-VSVg (10 μg), and CMVΔR8.9 (15 μg) with Lipofectamine 2000 (Invitrogen) according to the manufacturer's protocol. Two days later, supernatant was removed, filtered through a 0.45 μm sterile filter, and centrifuged at 25,000 rpm in an SW28 rotor at 4°C for 2 h. Supernatant was removed and the resulting pellet was resuspended in PBS, aliquoted, and frozen at −80°C. Lentiviral titers were determined by transduction of 10^5 HEK293T cells with serial dilutions of concentrated virus, followed by counting of GFP-positive cells after 3 d.

Hippocampal neurons for transduction and subsequent electrophysiology were prepared as previously described (Shin and Chetkovich, 2007). Neurons were infected at multiplicity of infection (MOI) of 5 at DIV 12. Immunocytochemistry of transduced neurons was performed

between DIV 16–21 as previously described with minor modification (Shin and Chetkovich, 2007). Briefly, neurons were fixed with 4% PFA/4% sucrose in PBS for 20 min at room temperature, permeabilized with PBS-T, and blocked with 3% NGS/PBS-T for 1 h. Neurons were stained with gp-anti GFP (1:1000), rab anti-TRIP8b (1:5000), and Hoechst stain (1:10,000) diluted in block solution, followed by 3 × 5 min PBS-T wash and staining with secondary antibodies (Alexa 488 goat α-gp, 1:2000, Invitrogen; Cy3 goat α-rab, 1:2000, Jackson ImmunoResearch). After 3 × 5 min PBS-T wash, coverslips were mounted on slides (Fisher) using Fluoromount-G (Southern Biotechnology Associates). To assess TRIP8b knockdown in neurons infected with lentivirus expressing either shControl or TRIP8b-sh4, DIV 10 hippocampal neurons were infected with equal titers of virus, followed by change of media the next day. After 11 d in culture, neurons were lysed and Western blotting performed as described. Membranes were probed with rab anti-TRIP8b and ms anti-tubulin. Experiments were performed three times demonstrating consistent results.

Electrophysiology

HEK293T electrophysiology. HEK293T cells were cotransfected with 1 μg of HCN1 cDNA plus 1 μg of TRIP8b isoform cDNA and 0.5 μg of EGFP cDNA using FuGENE 6 (Roche Applied Science) according to the manufacturers recommended protocol. In control conditions lacking TRIP8b isoforms 1.5 μg of EGFP cDNA was used. Transfected cells were detected by GFP fluorescence. For electrophysiological recording, cells were bathed in an extracellular solution containing (in mM) 145 NaCl, 10 KCl, 10 glucose, 10 HEPES, 2 $CaCl_2$, 1 $MgCl_2$ with a pH of 7.4 and an osmolarity of 312–315 mOsm. The intracellular, pipette solution consisted of (in mM) 135 K gluconate, 10 $MgCl_2$, 0.1 $CaCl_2$, 1 EGTA, 10 HEPES and 2 MgATP (added on experiment day) with a pH of 7.3 and an osmolarity of 295–305. Recording pipettes were pulled from thin-walled glass capillary tubes (World Precision Instruments) by a P-2000 laser puller (Sutter Instruments) and fire-polished with a microforge (Narishige) to a resistance of 1.5–3.5 MΩ when filled with intracellular solution. Whole-cell currents were acquired using an Axopatch 200-B (Molecular Devices) at 20 kHz, filtered at 1 kHz, capacitance compensated 70%, and analyzed off-line with pClamp 9.2 (Molecular Devices). For channel activation, cells were held at -40 mV and stepped to voltages ranging from -120 to -25 mV in 5 mV increments. Only cells in which a 3 GΩ seal or better was achieved were kept for analysis. No leak subtraction was used. The maximal current amplitudes were calculated as the difference between the current amplitude at the beginning of the voltage step (after the capacitive transient) and the current amplitude at the end of the voltage step (Chen et al., 2005) and normalized to the capacitance of the cell to calculate current density. Maximal tail current amplitudes were plotted against the voltage step applied and fitted to the sigmoidal Boltzmann equation $Y = Bottom + (Top-Bottom)/\{1+\exp[(V_{50}-X)/Slope]\}$ using Prism Software (GraphPad). All comparisons were made using unpaired Student's t tests with Welch's correction in the case of unequal variances with Prism.

Cultured hippocampal neurons. Conventional tight-seal (>3 GΩ) whole-cell patch-clamp recordings were made on visually identified hippocampal neurons in culture (neurons for infection studies were infected on DIV12; recording were performed after 6 d of infection) based on their size and somatodendritic morphology. External solution containing (in mM) 104 NaCl, 2.1 KCl, 20.1 $NaHCO_3$, 1.1 NaH_2PO_4, 1.7 $CaCl_2$, 0.8 $MgCl_2$, and 10.8 glucose bubbled continuously with carbogen (95% O_2 and 5% CO_2). For all voltage- and current-clamp recordings, patch electrodes were filled with internal solution containing (in mM) 112.1 K-MeSO$_4$, 4.2 KCl, 0.4 $CaCl_2$, 4.2 HEPES, 4.2 EGTA, 8.3 phosphocreatine disodium, 1.7 ATP-Mg, 0.4 GTP-Na; the pH was adjusted to 7.3. The liquid junction potential in our recording external solution was $\sim$8 mV and not corrected for. Signals were filtered at 1–4 kHz and digitized at 5–20 kHz with a Digidata 1322A (Molecular Devices). For current-clamp recordings, the amplifier bridge circuit was adjusted to compensate for electrode resistance and monitored. Electrode capacitance was also compensated. If series resistance increased $>20\%$ during recording, the data were discarded. Electrophysiological data collected was analyzed using ClampFit 9.1 (Molecular Devices), Igor Pro 6.0 (Wavemetrics).

Numerical data are expressed as medians and interquartile range because of the small sample size. Box plots were used for graphic presentation of the data. In data presented as box plots, the central line represents the median, the edges of the box represent the interquartile range, and the "whisker lines" show the extent of the overall distribution, excluding outliers (points $>1.5 \pm$ intraquatrile range). Statistical analysis was done with SigmaStat 3.5 (Systat Software) using nonparametric testing Mann–Whitney rank sum test for comparing between two groups or Kruskal Wallis ANOVA with Dunnet's *post hoc* for multiple group comparison. Probability (p) threshold for statistical significance was $p < 0.05$.

Pharmacological reagents and channel ligands. Reagents were purchased from Sigma except K-MeSO$_4$ (MP Biomedicals), GTP-Na (Roche Diagnostics).

Flow cytometry

HEK293T cells were transfected and maintained as described in the electrophysiology section. Methods and analyses used have been described previously (Lo et al., 2008). Briefly, cells were transfected with HA-tagged HCN1 plus a cDNA construct encoding a TRIP8b isoform or EGFP as a control. Nonpermeabilized cells were stained with ms α-HA primary antibody at a dilution of 1:250 to label surface HA and then were stained with goat α-ms secondary antibody conjugated to Alexa-647 (Invitrogen) at a dilution of 1:500. Cells were run in a Cyan ADP flow cytometer (Dakocytomation) at the Northwestern University Flow Cytometry Core facility. All events were recorded in the cytometer and data were analyzed off-line using FloJo and Prism software. Cells defined as positive in the cytometer were those whose fluorescence was $>99\%$ of the mock transfected (cells exposed to transfection reagent but no cDNA) control. Data are presented as the fluorescence index, which was calculated as the percentage of positive cells multiplied by the mean fluorescence of the cells in each transfection condition. The fluorescence indices for each condition were normalized to the control transfection condition (HCN1 plus GFP) and compared using a Student's unpaired t test with Welch's correction in the case of unequal variances.

Statistical analysis

Data are reported as SEM. Unless otherwise noted all error bars in figures represent SEM. Detailed statistical methods are described within the methods text above.

Results

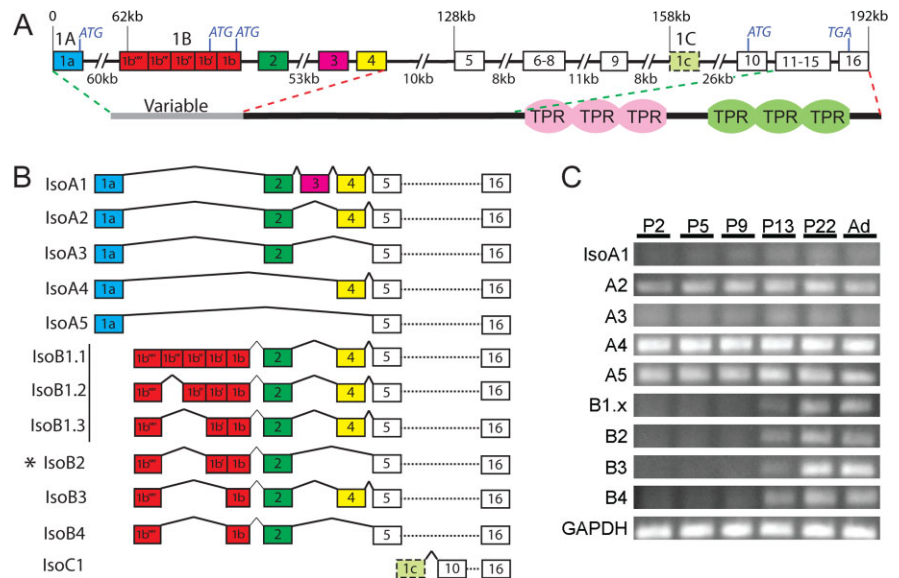### The N terminus of TRIP8b is alternatively spliced

At first glance, previous studies examining the molecular role of TRIP8b yielded seemingly contradictory results. An initial report characterizing TRIP8b found that overexpression of TRIP8b in AtT20 cells enhanced cAMP-induced secretion of ACTH (Chen et al., 2001b), suggesting a stimulatory effect of TRIP8b in vesicle trafficking and membrane fusion. However, Santoro et al. (2004) found that overexpression of TRIP8b in oocytes, HEK293 cells, and cultured neurons downregulated I_h and removed both HCN1 and HCN2 from the cell surface, indicating an inhibitory effect of TRIP8b on h channel trafficking. In addition to different *in vitro* models, an important difference between these two seemingly contradictory studies was the use of TRIP8b cDNA constructs based on different splicing of the gene encoding TRIP8b, *Pex5l*. This alternative splicing resulted in TRIP8b proteins with different sequences (Santoro et al., 2004). Therefore, we tested the notion that significant alternative splicing of TRIP8b existed in the brain, and that this alternative splicing governed the function of each resulting isoform in the regulation of channel function. We performed a survey of known expressed sequence tags (ESTs) for TRIP8b in brain and testis (the only tissues known to express the *Pex5l* transcript) and identified a number of different splice variants. Based on ESTs, *Pex5l* consists of at least three different alternative promoters (A–C), each with distinct 5′ untranslated regions and start codons, along with 15 other exons. RT-PCR was then performed using adult rat brain mRNA with

forward primers designed to flank predicted TRIP8b promoter regions and reverse primers located within exons included in known ESTs. This experiment revealed that only two of the promoters (A, B) were used in brain, and three of the 15 nonpromoter exons were alternatively spliced to generate 11 distinct mRNA species. These transcripts are predicted to encode nine unique TRIP8b isoforms in brain (Fig. 1B) that range from 567 to 650 aa in length and include the two TRIP8b isoforms used in the Chen et al. and Santoro et al. studies (which we have named TRIP8b_IsoA4 and TRIP8b_IsoB2, respectively) (supplemental Fig. 1, available at www.jneurosci.org as supplemental material). EST analysis and RT-PCR of testis mRNA demonstrated a unique transcript arising from a third promoter region (C) that includes seven exons from the 3′ region of *Pex5l*, which if translated, would produce a protein of 344 aa.

To better characterize alternative splicing of the transcripts encoding TRIP8b, we performed RT-PCR studies to look at the changes in *Pex5l* transcript splicing in the brain during development. We found that TRIP8b transcripts were expressed in both a constitutive and developmentally regulated manner (Fig. 1C) depending on the promoter region used. The first promoter region (A) generates five isoforms encoded by mRNA transcribed constitutively from birth, whereas four isoforms initiated by the second promoter (B) were encoded by 6 mRNA species that are upregulated at the end of the second postnatal week. Expression of two of the isoforms generated by the first promoter, TRIP8b_IsoA1 and TRIP8b_IsoA3, was extremely low compared with other isoforms (Fig. 1C). We thus focused our analysis on the other 7 TRIP8b isoforms expressed more abundantly in the brain. For simplification, we hereafter refer to individual isoforms by their identifying suffix (for example, TRIP8b_IsoB2 is thus abbreviated IsoB2).
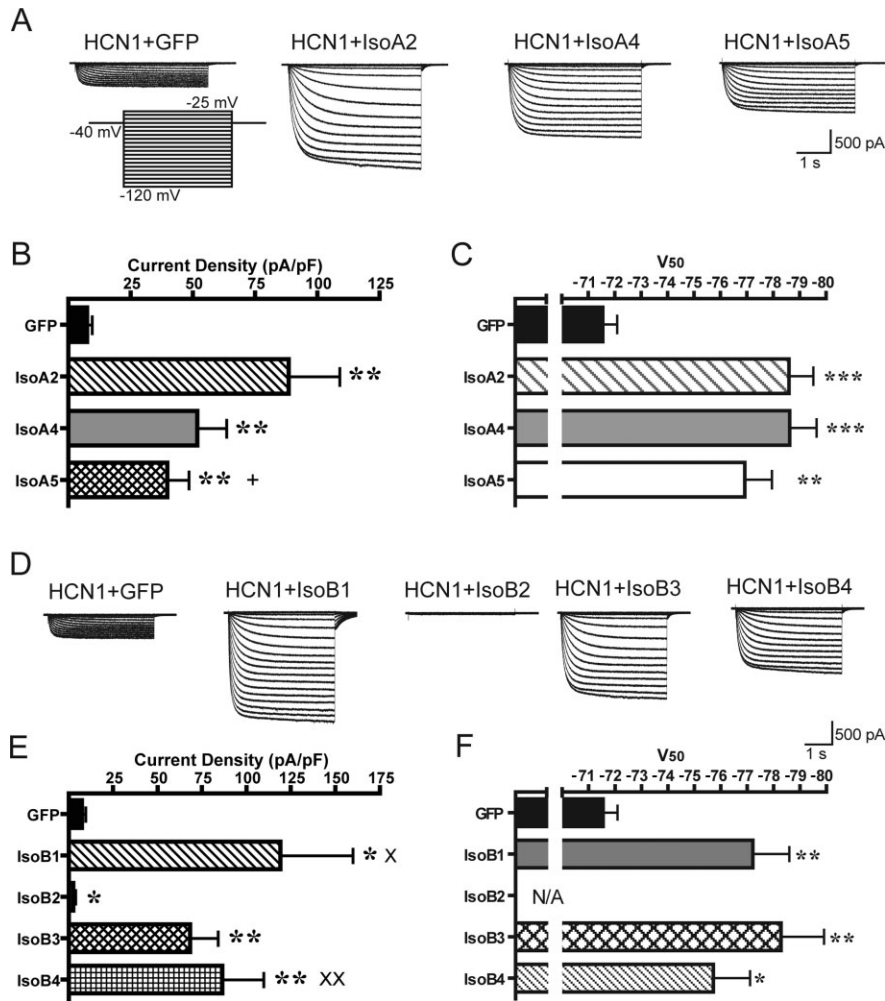
Isoform-specific effects of TRIP8b on the properties of I_h
We next explored whether alternatively spliced isoforms of TRIP8b differentially affect h channel currents. We thus recorded whole-cell currents under voltage-clamp from HEK293T cells coexpressing HCN1 and GFP without the addition of TRIP8b, or HCN1 and GFP plus each of the 7 most abundant TRIP8b isoforms. When HCN1 alone was expressed with GFP, transfected HEK293T cells exhibited slowly activating current on negative voltage steps followed by inward tail current after return to the holding voltage consistent with I_h (Fig. 2A). Such current was abolished after application of 5 mM cesium chloride to the recording bath (data not shown). The current density for the HCN1 transcript cotransfected with GFP at -110 mV was 7.50 ± 2.02 pA/pF ($n = 21$). The half-maximal voltage activation (V_{50}) was determined from a Boltzmann fit of the maximal tail current amplitude elicited after returning to a holding voltage of -40 mV after steps from -120 to -25 mV in 5 mV increments. The V_{50} obtained from cells cotransfected with HCN1 and GFP was -71.6 ± 0.5; $n = 4$ (Fig. 2A,C) consistent with previously reported values (Chen et al., 2001a). Coexpression of HCN1 with the abundant promoter A isoforms resulted in a robust increase in the current density (Fig. 2A,B). Specifically, cotransfection with IsoA5, an isoform that lacks the alternatively spliced exons 2 or 4, increased HCN1 current density at a -110 mV step to 39.8 ± 8.58 ($n = 19$, $p < 0.01$). Interestingly, cotransfection with IsoA2 or IsoA4 (which compared with IsoA5 includes exons 2 and 4, or exon 4, respectively) increased current density higher than IsoA5 (values at a -110 mV step for IsoA2: 88.5 ± 20.4 pA/pF, $n = 10$, $p < 0.01$ compared with GFP and IsoA5; for IsoA4: 51.9 ± 11.6 pA/pF, $n = 17$, $p < 0.01$ compared with GFP and IsoA5) (Fig. 2A,B). Together, these findings show that TRIP8b "A" isoforms increase the magnitude of HCN1-mediated current, and suggest exon 4 enhances this effect. All promoter A-containing TRIP8b isoforms caused a similar hyperpolarizing shift in voltage dependence of channel activation when coexpressed with HCN1 (Fig. 2C). Specifically, the Boltzmann fit of tail current amplitudes obtained when HCN1 was cotransfected with IsoA2, IsoA4, and IsoA5 respectively yielded a V_{50} of -78.6 ± 1.1 mV ($n = 4$; $p < 0.001$), -78.6 ± 1.0 mV ($n = 8$; $p < 0.001$) and -76.9 ± 1.0 ($n = 9$, $p < 0.01$; for magnified tail currents and individual Boltzmann plots see supplemental Fig. 2, available at www.jneurosci.org as supplemental material). We then examined the effects of the 4 TRIP8b isoforms originating from promoter B. These isoforms include either exon 2 or both exon 2 and exon 4, and also differ in the length of exon 1b. Compared with current when HCN1 was cotransfected with GFP alone (current density of 7.5 ± 2.02 pA/pF, $n = 21$), cotransfection with exons 2- and 4-containing IsoB1 dramatically increased HCN1 current density (119 ± 40.6 pA/p, $p < 0.05$, $n = 10$) (Fig. 2D,E). However, IsoB2, which differs from IsoB1 only in lacking

Figure 1. Alternative splicing of the TRIP8b N terminus is regulated during development. **A**, *Pex5l*, the gene encoding TRIP8b, spans 192 kb (in mice) and contains three alternative promoters (1A, 1B, and 1C), three alternatively spliced exons (2, 3, and 4), and 12 other exons. The protein encoded by most brain isoforms includes a variable N terminus and conserved C terminus that consists of six TPR domains. In the gene schematic, large introns are indicated by the line breaks, and alternative start (ATG) and the stop codon (TGA) are also noted. **B**, RT-PCR analysis of mRNA isolated from rat hippocampus using primers designed from ESTs to flank alternatively spliced regions identified 12 different splice isoforms. Eleven of twelve are expressed in the brain, whereas one splice isoform, TRIP8b_IsoC1, is expressed in testis. Asterisk indicates isoform used in study by Santoro et al. (2004). **C**, RT-PCR of hippocampal mRNA isolated from developing rats on postnatal day 2, 5, 9, 13, 22, and from adult (Ad) rats using PCR primers designed to amplify specific splice isoforms. Although TRIP8b_IsoB1.1, 1.2, and 1.3 represent three distinct mRNA species, they are predicted to encode one protein and a primer set amplifying exons common to all three (B1.x) was used. Glyceraldehyde 3-phosphate dehydrogenase (GAPDH) was detected as a loading control.

Figure 2. TRIP8b isoforms increase or decrease I_h peak current in HCN1 cotransfected HEK293T cells depending on isoform identity. **A**, Representative electrophysiological traces elicited from cells voltage clamped at a holding voltage of -40 mV and stepped from -125 to -25 mV with 5 mV increments from cells cotransfected with HCN1 and equimolar amounts of GFP, IsoA2, IsoA4, or IsoA5, respectively. **B**, Current density obtained from normalizing the peak current amplitude from step to -110 mV to the cell capacitance demonstrates that the presence of promoter A-containing TRIP8b isoforms alter h channel current in HEK293T cells. **C**, Cotransfection of HCN1 with IsoA2, IsoA4, and IsoA5 caused a hyperpolarizing shift in the half-maximal voltage of activation (V_{50}) of HCN1 when compared with control cotransfection with GFP (**$p < 0.01$; ***$p < 0.001$; $+p < 0.05$ when compared with HCN1 with IsoA2 cotransfection). **D**, Representative electrophysiological traces obtained from cells transfected with HCN1 and GFP or with promoter B-containing TRIP8b isoforms have variable effects of TRIP8b on HCN1 current. **E**, Comparison of current density obtained by normalizing peak current amplitude at step to -110 mV to cell capacitance demonstrates that cotransfection of HCN1 with promoter B-containing TRIP8b isoforms alter h channel current density and caused a hyperpolarizing shift in the voltage of half-maximal activation when compared with the GFP-transfected control (**F**). Because of the extremely small size of the current obtained when HCN1 was cotransfected with IsoB2, the V_{50} could not be measured (*$p < 0.05$; **$p < 0.01$ when compared with HCN1 cotransfected with GFP; $^{XX}p < 0.01$ when compared with HCN1 cotransfected with IsoB2).

exon 4, significantly downregulated I_h (2.62 ± 1.08 pA/pF, $p < 0.05$, $n = 10$) (Fig. 2 D,E). In contrast, when exon 2 was paired with the shorter 1b exon as in IsoB4, there was significant upregulation of h channel current when compared with current density recorded from cells cotransfected with HCN1 and GFP alone (86.4 ± 21.3 pA/pF, $p < 0.05$, $n = 9$) (Fig. 2 D,E), as well as when compared with cells cotransfected with HCN1 and IsoB2 ($p < 0.01$) (Fig. 2 D,E). These results indicate that the unique 25 aa of the longer 1b' exon, when present in isoforms that contain exon 2 but not exon 4, dominantly exert a repressive effect of TRIP8b on HCN1-mediated current. Interestingly, HCN1 current-promoting effects of exon 4 appeared to be able to overcome any negative effects of exon 1b' as current density obtained from cells cotransfected with HCN1 and IsoB1 was greater than from cells

cotransfected with HCN1 and IsoB2 ($p < 0.05$, $n = 10$) (Fig. 2 D,E). However, in the presence of the shorter 1b promoter, exon 4 in TRIP8b did not significantly alter the HCN1-mediated current density (IsoB3 vs IsoB4, $p = 0.507$, $n = 12$) (Fig. 2 D,E).

In addition to effects on HCN1 current density, the voltage sensitivity of HCN1-mediated current was altered in the presence of the promoter B-containing TRIP8b isoforms. Similar to the TRIP8b promoter A-containing isoforms, the half-maximal voltage of activation derived from a Boltzmann fit of the tail current amplitude was shifted in a hyperpolarizing direction in the presence TRIP8b (HCN1 cotransfected with GFP, -71.6 ± 0.5 mV, $n = 4$; HCN1 with IsoB1, -77.2 ± 1.4 mV, $p < 0.01$, $n = 7$; HCN1 with IsoB3, -78.3 ± 1.6 mV, $p < 0.01$, $n = 6$; HCN1 with IsoB4, -75.7 ± 1.4 mV, $p < 0.05$, $n = 6$, Fig. 2 F) (for magnified tail currents and individual Boltzmann plots, see supplemental Fig. 2, available at www.jneurosci. org as supplemental material). It should also be noted that the currents obtained from cells cotransfected with HCN1 and IsoB2 were too small to measure the tail current amplitude beyond the noise of the system (~ 5 pA) and were therefore not included in the analysis. Together, our data show that when coexpressed with HCN1 in HEK293T cells, splice variants of TRIP8b cause a hyperpolarizing shift in activation voltage of h channels, but that TRIP8b isoforms differentially upregulate or downregulate h current density. These results suggest that the TRIP8b alternative promoters and alternatively spliced exons encode distinct functional domains that allow TRIP8b to have dramatically different effects on HCN1-mediated current density.

Alterations in I_h are largely attributable to TRIP8b effects on HCN1 surface trafficking

TRIP8b isoforms could upregulate or downregulate HCN1-mediated I_h by alter-

ing the channel conductance or by changing the number of channels expressed on the cell surface. To directly test the latter possibility, we first created an HCN1 construct (HCN1-HA) tagged with the HA-epitope on the extracellular domain of the channel between transmembrane regions S3 and S4 (Fig. 3A). This construct was efficiently expressed on the surface membrane of transfected COS7 cells (Fig. 3B) and demonstrated hyperpolarization-activated current in HEK293T cells (data not shown). We then performed flow cytometry of nonpermeabilized HEK293T cells transfected with HCN1-HA and the TRIP8b isoforms previously studied by electrophysiology. When cotransfected with the control protein, GFP, flow cytometric studies revealed that HCN1-HA was expressed on the cell surface and that staining of the HA tag could be detected beyond the signal of

mock-transfected control (Fig. 3C,D). For each experiment, all flow cytometric data were normalized to the value of the fluorescence index of the control condition in which HCN1-HA was cotransfected with only GFP (set at a fluorescence index of 1). During cotransfection with the promoter A-containing isoforms, there was an increase in the HCN1-HA fluorescence index compared with control (3.47 ± 0.40, $n = 6$, $p < 0.01$ for IsoA2; 3.41 ± 0.58, $n = 6$, $p < 0.01$ for IsoA4; 1.64 ± 0.22, $n = 6$, $p < 0.05$ for IsoA5) (Fig. 3C,E), which correlated with the current density data (Fig. 2). IsoB2, which decreased HCN1 current density in electrophysiological studies, reduced the fluorescence index of surface-stained cells (0.35 ± 0.02, $n = 6$, $p < 0.001$) (Fig. 3D,F). Also in correlation with the electrophysiological results, cotransfection of IsoB3 and IsoB4 increased the surface HCN1-HA flow cytometric signal (2.97 ± 0.21, $n = 6$, $p < 0.001$ for IsoB3 and 2.12 ± 0.4, $n = 6$, $p < 0.05$ for IsoB4) (Fig. 3D,F), whereas, unexpectedly, cotransfection of HCN1-HA with IsoB1 did not result in a statistically significant increase in surface HCN1-HA signal (1.45 ± 0.23, $n = 3$, $p = 0.19$) (Fig. 3D,F). Together, the generally excellent concordance of the effects of individual TRIP8b isoforms on current density and surface expression supports the notion that changes in the current density are mediated by altered surface expression of the HCN1 channels.

In addition, because the HCN1-HA fluorescence index obtained from samples cotransfected with IsoB3 was greater than in samples cotransfected with IsoB1, and that from IsoB4 was greater than IsoB2, the flow cytometry data support a role for the longer 1b′ exon of IsoB1 and IsoB2 in removing HCN1 channels from the cell surface.

As another measure to evaluate effects of TRIP8b isoforms on HCN1 membrane expression, we assayed HCN1 surface expression by biochemical methods. In these studies, we performed immunoprecipitation of the HA-tag in nonpermeabilized HEK293T cells coexpressing HCN1-HA and three TRIP8b isoforms observed to have different effects on HCN1-mediated current density. We found that cotransfection of HCN1-HA with IsoA4 or IsoB3, isoforms that increased HCN1 current density, significantly increased HCN1-HA surface expression when compared with HCN1-HA cotransfected with GFP alone, whereas IsoB2, which decreased HCN1 current density in electrophysiological studies, strongly reduced surface expression of HCN1-HA (values were normalized to HCN1-HA plus GFP: HCN1-HA plus GFP, 1.00 ± 0.12; HCN1-HA plus IsoA4, 2.04 ± 0.27; HCN1-HA plus IsoB2, 0.050 ± 0.04; HCN1-HA plus IsoB3, 1.69 ± 0.08; $n = 3$–4; $p < 0.05$ for GFP vs IsoB3; $p < 0.01$ for GFP vs IsoA4 and
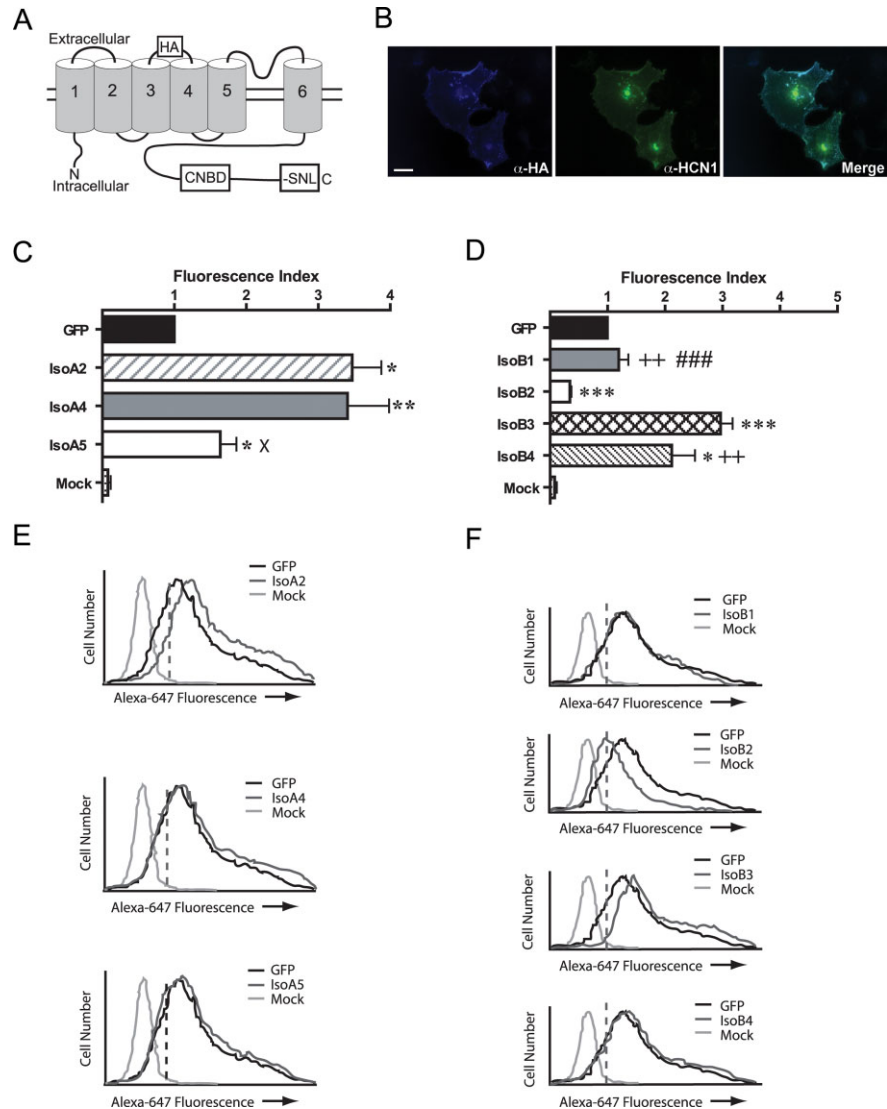

Figure 3. TRIP8b isoforms bidirectionally modify HCN1 protein surface expression as determined by flow cytometry. **A**, Schematic of HCN1 construct illustrating the location of an extracellular HA epitope between transmembrane segments 3 and 4 (this construct is hereafter referred to as HCN1-HA). **B**, COS7 cells were transfected with HCN1-HA and stained without permeabilization for HA (blue) followed by permeabilization and staining for HCN1 (green), demonstrating that the HCN1-HA construct is expressed on the cell surface (enhanced HA staining at margins of cell). **C**, Cotransfection of HCN1-HA with promoter A-containing TRIP8b isoforms resulted in an increase in surface HA immunofluorescence (*$p < 0.05$, **$p < 0.01$, when compared with HCN1-HA cotransfected with GFP; $^X p < 0.05$ when compared with HCN1-HA cotransfected with IsoA2). **D**, Cotransfection of HCN1-HA with promoter B-containing TRIP8b isoforms resulted various changes in surface HA immunofluorescence (*$p < 0.05$, ***$p < 0.001$, when compared with HCN1-HA cotransfected with GFP; $^{++} p < 0.01$ when compared with cells cotransfected with HCN1-HA and IsoB2; $^{###} p < 0.001$ when compared with cells cotransfected with HCN1-HA and IsoB3). **E**, Representative flow cytometric histograms obtained when HCN1-HA was cotransfected with GFP or IsoA2, IsoA4 and IsoA5 and GFP or IsoB1, IsoB2, IsoB3, and IsoB4 (**F**). Dashed line indicates location of gate for positive cells. Note, x-axes were plotted on a log scale. Scale bar: **B**, 20 μm.

IsoB2, one-way ANOVA with Dunnett's post test) (Fig. 4A,B). These data demonstrate that TRIP8b can control h channel current density by upregulation or downregulation of h channel surface expression, although other mechanisms such as effects on single-channel conductance may also be involved.

Dual interaction domains in TRIP8b and HCN1 molecules
Prior studies have shown that the interaction between TRIP8b and HCN subunits requires a C-terminal portion of TRIP8b, as well as the C-terminal 3 aa of HCN subunits (Santoro et al., 2004). Because this C-terminal portion of TRIP8b is present in all brain splice isoforms, we reason that all TRIP8b isoforms bind to
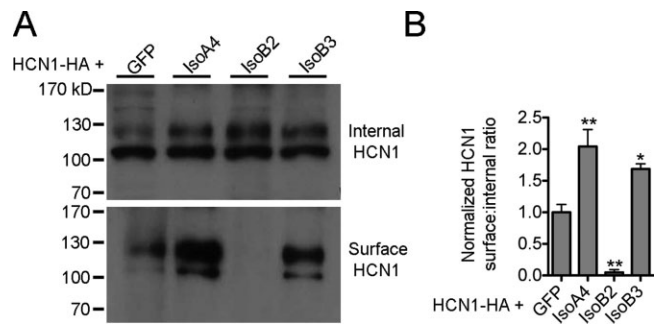
Figure 4. TRIP8b isoforms A4, B2, and B3 alter amount of surface HCN1 protein. *A*, *B*, HEK293T cells were cotransfected with HCN1-HA and GFP, IsoA4, IsoB2, or IsoB3, and surface fraction of HCN1 was assessed by immunoprecipitation of the HA-epitope followed by Western blotting of surface and internal HCN1 fractions. Quantification of HCN1 surface to internal ratio, normalized to HCN1-HA plus GFP surface to internal ratio, revealed that relative surface expression of HCN1 was significantly increased by IsoA4 and IsoB3, and decreased by IsoB2 ($n = 3–4$; *$p < 0.05$, **$p < 0.01$ when compared with HCN1-HA plus GFP cotransfection; 1-way ANOVA with Dunnett's post test). Film exposure for the internal and surface fraction was identical. Loading for internal HCN1 was 10% of total surface fraction immunoprecipitated. Upper and lower bands represent glycosylated and nonglycosylated HCN1, respectively, demonstrating that surface HCN1 overwhelmingly consists of glycosylated HCN1, as previously described for both HEK cells and neurons (Much et al., 2003; Zha et al., 2008). Molecular mass markers are shown in kilodaltons (kD). Error bars indicate SEM.

HCN1 subunits. However, the observation that TRIP8b influenced h channel gating independently of effects on surface expression suggested the possibility that the interaction between TRIP8b and h channel subunits might involve more than one site of interaction. We, therefore, sought to determine what regions of TRIP8b are necessary for binding to h channels. We first investigated the interaction between HCN1 and TRIP8b by yeast two-hybrid analysis of different domains of either protein. As expected, we found that the interaction of TRIP8b with the final 133 aa of HCN1 was interrupted by removal of the C-terminal 3 aa ending of HCN1 (–SNL) (Fig. 5*B*). Intriguingly, HCN1(386–907), which comprises the entire intracellular tail except the –SNL ending, restored binding to TRIP8b, suggesting a second binding site independent of the final 3 aa. We mapped this binding further to within HCN1(386–591), a region encompassing the cyclic nucleotide-binding domain (CNBD), a domain common to all h channel subunits that confers channel responsiveness to cyclic nucleotides (Wainger et al., 2001). We next explored which region(s) of the TRIP8b molecule were involved in the interaction with the two distinct sites of HCN1 (Fig. 5*C*). Prior studies have demonstrated that the TRIP8b C terminus is required for interaction with HCN1 and other binding partners (Amery et al., 2001; Chen et al., 2001b; Santoro et al., 2004). The TRIP8b C terminus contains two sets of three tetratricopeptide repeat (TPR) domains, which mediate protein-protein interactions in many proteins (D'Andrea and Regan, 2003). As expected, a full-length TRIP8b construct, IsoA4, bound to both HCN1(386–591) (hereafter referred to as $HCN1_{CNBD}$) and HCN1(778–910) (hereafter referred to as $HCN1_{C\text{-}term}$). $HCN1_{CNBD}$ and $HCN1_{C\text{-}term}$ both bound to TRIP8b constructs in which 150 [IsoA4(151–602)] or 200 [IsoA4(201–602)] amino acids were deleted from the N terminus. However, IsoA4(259–602) bound to $HCN1_{C\text{-}term}$ but not $HCN1_{CNBD}$, indicating that $HCN1_{CNBD}$ binding required amino acids 201–259. Interaction with $HCN1_{C\text{-}term}$ resembled traditional TPR domain-containing protein interaction with tripeptide motifs, as neither TRIP8b TPR set I [IsoA4(259–450)] nor set II [IsoA4(451–602)] alone was sufficient for interaction. In contrast, interaction with the

$HCN1_{CNBD}$ did not require both sets of TPR domains, but did require the complete TPR set I. $HCN1_{CNBD}$ interacted with TRIP8b IsoA4(1–451) but not TRIP8b IsoA2(1–374). Together, these results indicated a mechanism of dual binding of TRIP8b with HCN1, whereby the combination of both sets of TPR domains is required to bind to the C-terminal tripeptide of HCN1 (–SNL), whereas the first TPR set with 58 amino acid residues N-terminal to the TPR domains was required to bind to $HCN1_{CNBD}$. We next confirmed this dual interaction between HCN1 and TRIP8b in mammalian HEK293T cells by coimmunoprecipitation. We first demonstrated that the alternatively spliced region of TRIP8b was not required for binding to HCN1 or HCN2, as both full-length TRIP8b and ΔN-IsoA4, which lacks any of the variably included exons 1–4, were immunoprecipitated by HCN1 and HCN2 with equal efficiency (Fig. 5*D*). We then sought to confirm which regions of TRIP8b mediate the dual interaction with HCN1. Full-length TRIP8b immunoprecipitated both full-length HCN1 and an HCN1 construct lacking the last 3 aa, HCN1Δ3 (Fig. 5*E*) (for characterization of gp α-TRIP8b antibody used here, see supplemental Fig. 3, available at www.jneurosci.org as supplemental material), consistent with bipartite interaction. Interaction of GFP-tagged IsoA4(259–602) with HCN1 required the HCN1 C-terminal peptide, consistent with yeast two-hybrid data and canonical TPR domain-ligand interactions (Fig. 5*F*) (for characterization of GFP antibodies, see supplemental Fig. 3, available at www.jneurosci.org as supplemental material). Furthermore, we found that GFP-tagged IsoA4(201–602) bound HCN1Δ3, confirming the importance of the 58 amino acid residues N-terminal to the TRIP8b TPR domains for the second site of HCN1 binding (Fig. 5*G*). Together, these studies show that TRIP8b interacts with HCN1 at two distinct sites requiring two specific regions of the TRIP8b molecule.

TRIP8b isoforms differentially alter trafficking of HCN1 in neurons
Because different isoforms of TRIP8b elicited different effects on HCN1-mediated current and surface expression in HEK293T cells, yet all TRIP8b isoforms bind to HCN1, we tested whether the differential structure of the isoforms might govern their effects on h channel trafficking and subcellular localization in neurons. We transfected cultured primary hippocampal neurons with GFP-tagged HCN1 and IsoA4 or IsoB2, isoforms which either up- or downregulate the surface trafficking of HCN1 (Figs. 2–4), respectively. Although both TRIP8b isoforms were colocalized with HCN1-GFP, the subcellular localization of HCN1-GFP differed dramatically between the two isoforms (Fig. 6*A–F*). With IsoA4, HCN1-GFP exhibited perimembranous localization and was diffusely distributed in dendrites (Fig. 6*A–C*), a distribution similar to that found previously for native HCN1 in primary hippocampal neurons (Shin and Chetkovich, 2007). In contrast, cotransfection with IsoB2 led to punctate distribution of HCN1-GFP in the soma and dendrites (Fig. 6*D–F*), resembling the subcellular punctate distribution observed during coexpression of IsoB2 with GFP-tagged HCN2 in HEK293 cells (Santoro et al., 2004). Interestingly, IsoA4 and IsoB2 were both diffusely localized throughout the neuron when transfected alone (without HCN1-GFP) (see supplemental Fig. 4, available at www.jneurosci.org as supplemental material) and were highly colocalized with MAP-2, indicating that TRIP8b was mainly confined to the dendrites and cell body. As discussed above, the distribution of IsoB2 differed markedly from its localization when cotransfected with HCN1-GFP, suggesting that the subcellular trafficking of TRIP8b depends on whether it is bound to
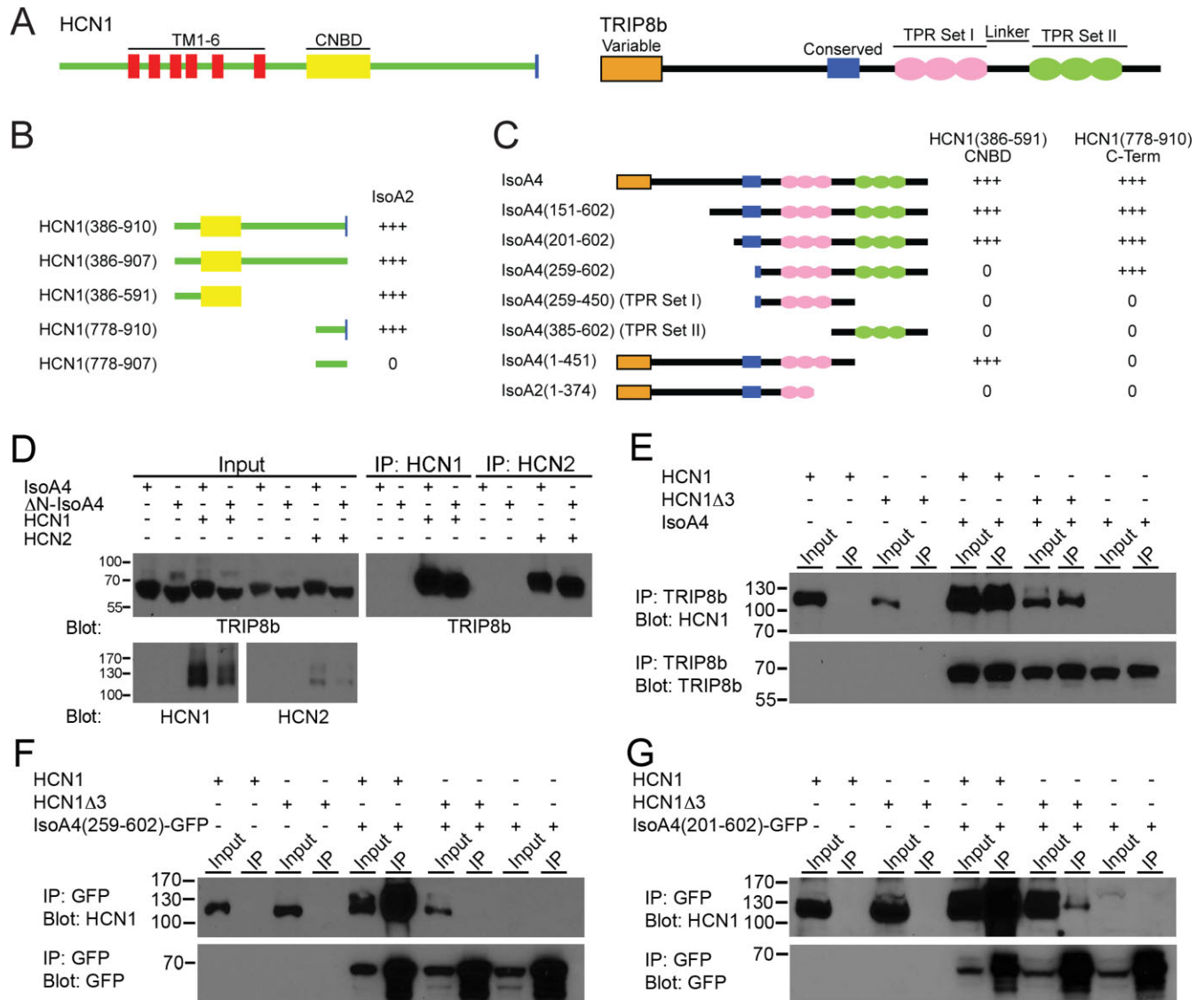
Figure 5. TRIP8b interaction with HCN1 is independent of TRIP8b alternative splicing and is bipartite. ***A***, Representation of full-length HCN1 bait and TRIP8b prey used for yeast two-hybrid directed interaction assays. TM, Transmembrane. ***B***, Directed yeast two-hybrid interactions with the intracellular C-terminal tail of HCN1 and full-length TRIP8b (IsoA2) revealed that TRIP8b binding to the final 133 aa of HCN1 [HCN1(778–910)] requires the –SNL. TRIP8b binding to a longer region of the HCN1 intracellular tail was independent of the –SNL tripeptide but required the HCN1 CNBD. +++ denotes positive interaction; 0 denotes no interaction. ***C***, The HCN1 CNBD [HCN1(386–591), HCN1$_{CNBD}$] and HCN1 C-terminal 133 aa [HCN1(778–910), HCN1$_{C-term}$] were used in yeast two-hybrid directed interactions with regions of the TRIP8b protein and showed that binding to HCN1$_{CNBD}$ and HCN1$_{C-term}$ is mediated by distinct regions of TRIP8b. ***D***, HEK293T cells were transfected with IsoA4 or a construct lacking the alternatively spliced N terminus of TRIP8b, IsoA4(43–602) (ΔN-IsoA4), and HCN1 or HCN2. Immunoprecipitation of HCN1 or HCN2 revealed strong coimmunoprecipitation of IsoA4 or ΔN-IsoA4, demonstrating that the alternatively spliced region of TRIP8b is not required for interaction with HCN1 or 2. Input is 12.5% of total lysate immunoprecipitated. ***E–G***, HEK293T cells transfected with HCN1 or HCN1(1–907) (HCN1Δ3) and IsoA4, IsoA4(259–602)-GFP, or IsoA4(201–602)-GFP. Cell lysates were prepared and full-length TRIP8b (***E***) or GFP (***F***, ***G***) was immunoprecipitated, revealing that amino acids 201–259 of TRIP8b are required for binding to HCN1Δ3. Input is 5% of total lysate immunoprecipitated. Molecular mass markers are shown in kilodaltons (kD).

cargo. These results indicate that expression of TRIP8b can lead to a dramatic change in HCN1 subcellular localization, and that this effect is isoform-dependent.

The expression pattern of TRIP8b splice variants *in vivo*
Because specific isoforms of TRIP8b appeared to have important consequences for HCN1 surface expression, localization, and function, we reasoned that the distribution of these isoforms within the brain may govern HCN1 function in a regional and cell-specific manner. Individual TRIP8b isoforms contain combinations of shared exons (and thus shared markers for identification). Whereas detection of proteins corresponding to individual isoforms *in vivo* is not technically feasible (with the exception

of IsoA5, see below), detection of the exons within groups of isoforms expressed *in vivo* is possible. Therefore, we examined the distribution of the following TRIP8b isoforms containing selected combinations of exons within specific brain regions: (1) isoforms containing exon 2, (2) those containing exon 4, and (3) the single isoform, IsoA5, lacking both exon 2 and exon 4 (which could be identified specifically by the presence of the exon 1a-5 splice junction). We generated antibodies against IsoA5 and the TRIP8b exon 2 and exon 4 epitopes and verified their specificity in lysates from transfected HEK293T cells (Fig. 7*A*). Immunoblotting of adult rat hippocampal lysates demonstrated that the exon-specific antibodies detected bands at ~65 kDa, consistent with the predicted size of TRIP8b isoforms (Fig. 7*B*). To confirm
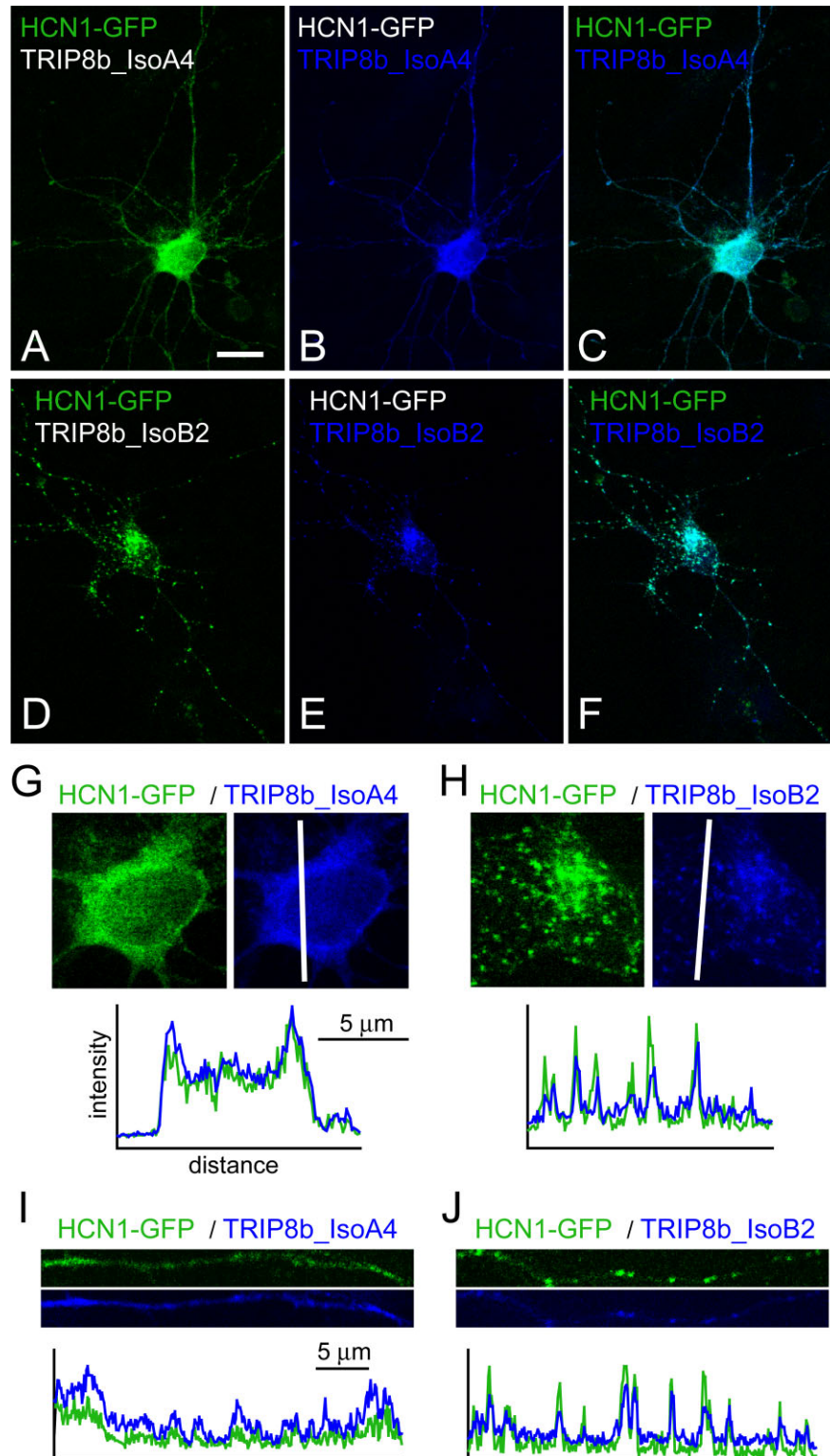
Figure 6. Isoforms of TRIP8b alter the trafficking of HCN1 in cultured hippocampal neurons. **A–F**, Constructs encoding HCN1-GFP and IsoA4 (**A–C**) or HCN1-GFP and IsoB2 (**D–F**) were transfected into hippocampal neurons which were then fixed at day 10 *in vitro*, stained with antibody to total TRIP8b (blue), and visualized using confocal microscopy. HCN1 was visualized directly by GFP fluorescence (green). Merged images are shown in **C** and **F**. **G**, **H**, Top panels are higher magnification of single z-slices of somata from neurons shown in **A–F**. Bottom panels are line plots of staining intensity along the white line shown in top panels that was drawn across the soma and reveal that HCN1 colocalizes with both isoforms of TRIP8b. Whereas HCN1-GFP is localized in a perimembranous distribution when cotransfected with IsoA4, the distribution of this channel is punctate when cotransfected with IsoB2. **I**, **J**, Top panels are higher magnification of single z-slices of dendrites of cells shown in **A–F**. Bottom panels are line plots along the length of the dendrite demonstrating a diffuse distribution of HCN1-GFP in neurons cotransfected with IsoA4, whereas HCN1-GFP in neurons cotransfected with IsoB2 appears punctate. Scale bar: (in **A**) **A–F**, 10 μm.

that these exon-specific antibodies recognized TRIP8b, we immunoprecipitated total TRIP8b from adult rat hippocampus followed by immunoblotting with exon-specific antibodies, showing that all three antibodies specifically recognized TRIP8b (Fig. 7C). Finally, these antibodies were efficient for immunoprecipitation, as they effectively cleared their epitope from supernatants of brain extracts as demonstrated by immunoblotting (Fig. 7D). These results demonstrate that TRIP8b exon-specific antibodies can be used to probe the distribution of specific TRIP8b isoforms within the brain.

Western blotting total protein lysates of brain extracts demonstrated that the abundance of total and specific exon-containing TRIP8b isoforms varied by brain region (see supplemental Fig. 5, available at www.jneurosci.org as supplemental material). We first performed Western blotting from protein lysates generated from cerebellum (Cb), cortex (Ctx), hippocampus (Hc), and "subcortex" (thalamus and striatum; Sub). In general, the cerebellum expressed less total TRIP8b when compared with cortex, hippocampus, and subcortex. Expression of IsoA5 appeared relatively evenly distributed throughout these four brain regions, whereas isoforms containing exon 2 and exon 4 were variably distributed. These data suggest that differential expression of TRIP8b isoforms could lead to brain region-specific differences in h channel function.

We next sought to determine the relative abundance of the alternatively spliced TRIP8b isoforms *in vivo* by using exon-specific immunoprecipitation from total lysate prepared from adult rat hippocampus and whole brain. In these experiments, we took advantage of the observation that all three groups of exon-specific isoforms were detectable in hippocampal extracts, and the fact that the exon-specific antibodies were efficient for immunoprecipitation (Fig. 7D). After immunoprecipitation, immunoblotting the immunoprecipitate and supernatant for total TRIP8b demonstrated that most hippocampal (Hc, top panel) and whole brain (WB, bottom panel) TRIP8b was immunoprecipitated and cleared from the supernatant by the exon 1a-5 and exon 4 antibodies (Fig. 8A), whereas a minor amount of TRIP8b was immunoprecipitated by exon 2 antibody, detectable on longer exposure of Western blots (Fig. 8A'). Because the α-Ex 2 antibody was efficient at immunoprecipitating exon 2-containing isoforms (Figs. 7D, 8B), these results suggested that most hippocampal and whole-
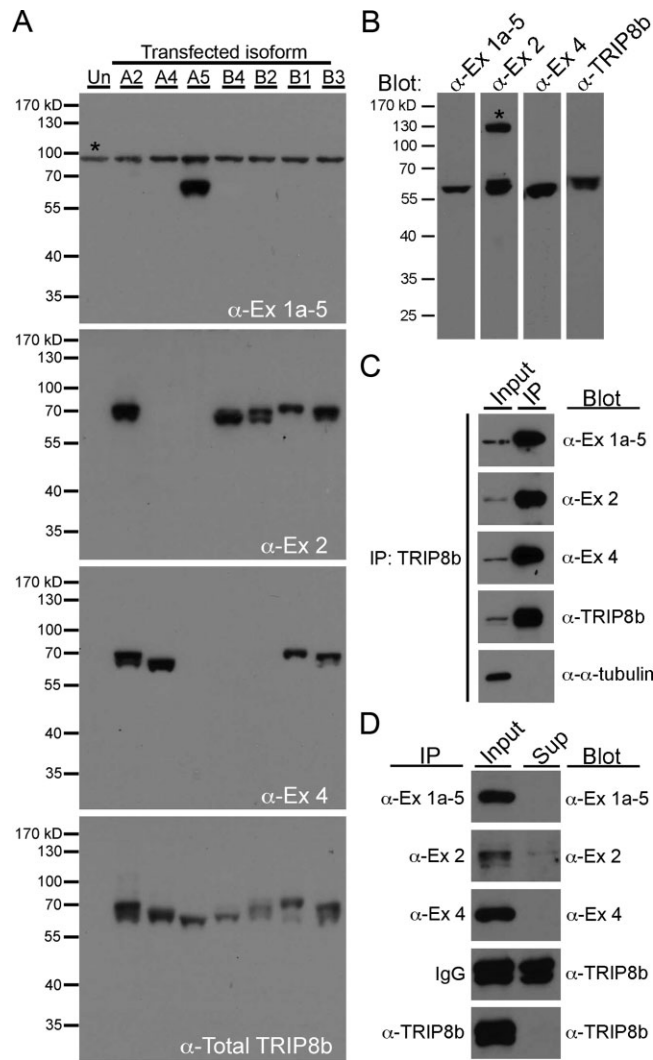
Figure 7. Exon-specific TRIP8b antibodies recognize TRIP8b isoforms and are effective for immunoprecipitation. ***A***, HEK293T cells were transfected with cDNAs encoding different TRIP8b splice isoforms. Immunoblotting cell lysates with exon-specific TRIP8b antibodies and total TRIP8b antibody demonstrates a band at the predicted molecular weight of ∼65–70 kDa only from cells expressing an isoform containing the appropriate epitope. Asterisk indicates a cross-reactive band not present in brain extracts (see ***B***). ***B***, Immunoblotting from hippocampal lysates with exon-specific TRIP8b antibodies and total TRIP8b antibody demonstrates bands at the predicted molecular weight of ∼65–70 kDa. A nonspecific band was also detected by α-Ex 2 (asterisk), which is not present during immunoprecipitation of total TRIP8b followed by immunoblotting for exon 2 (data not shown). ***C***, Antibodies to total TRIP8b were used for immunoprecipitation from adult rat hippocampus followed by immunoblotting with the indicated antibodies, demonstrating that all exon-specific antibodies recognize TRIP8b. α-Tubulin was not immunoprecipitated and served as a control for nonspecific protein interaction. Input is 5% of total lysate immunoprecipitated. ***D***, TRIP8b antibodies were used for immunoprecipitation (IP) from hippocampal lysates, and equal amounts of both input and supernatant (Sup) were immunoblotted with the indicated antibody. Molecular mass markers are shown in kilodaltons (kD).

brain TRIP8b lacked exon 2. The isoforms lacking exon 2 are IsoA4 (predicted to be recognized by exon 4 antibody) and IsoA5 (predicted to be recognized by 1a-5 antibody); thus, our data indicate that these two isoforms are the predominant isoforms not only in hippocampus but also in the entire brain. This conclusion is further supported by the observation that antibody to total TRIP8b detects a doublet in four different brain regions (see supplemental Fig. 5, available at www.jneurosci.org as supplemental material), consistent with the predicted 67 kd and 63 kd sizes of IsoA4 and IsoA5, respectively. Furthermore, the exon 1a-5 or exon 4 antibody immunopre-
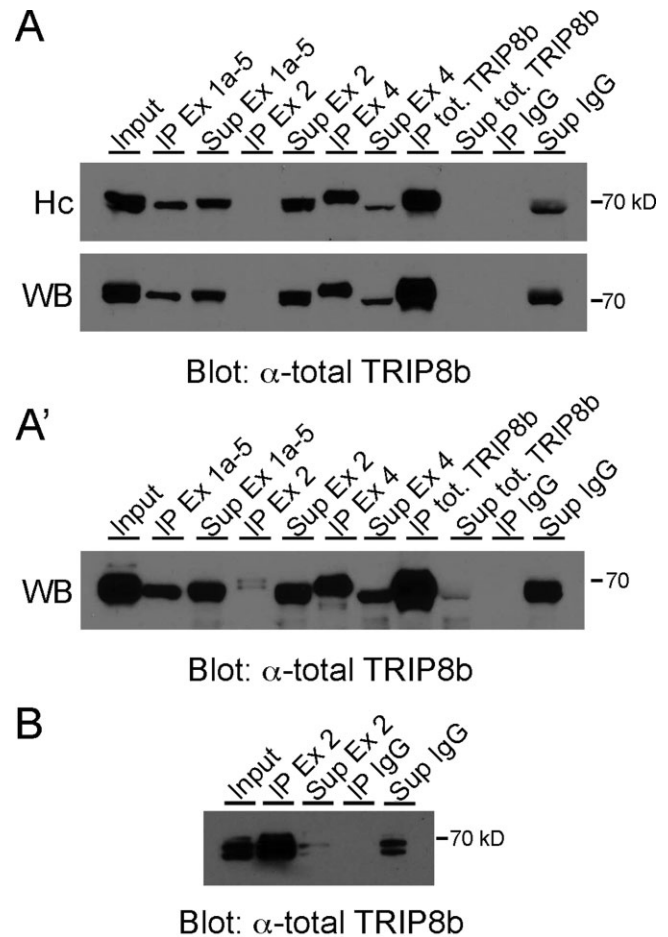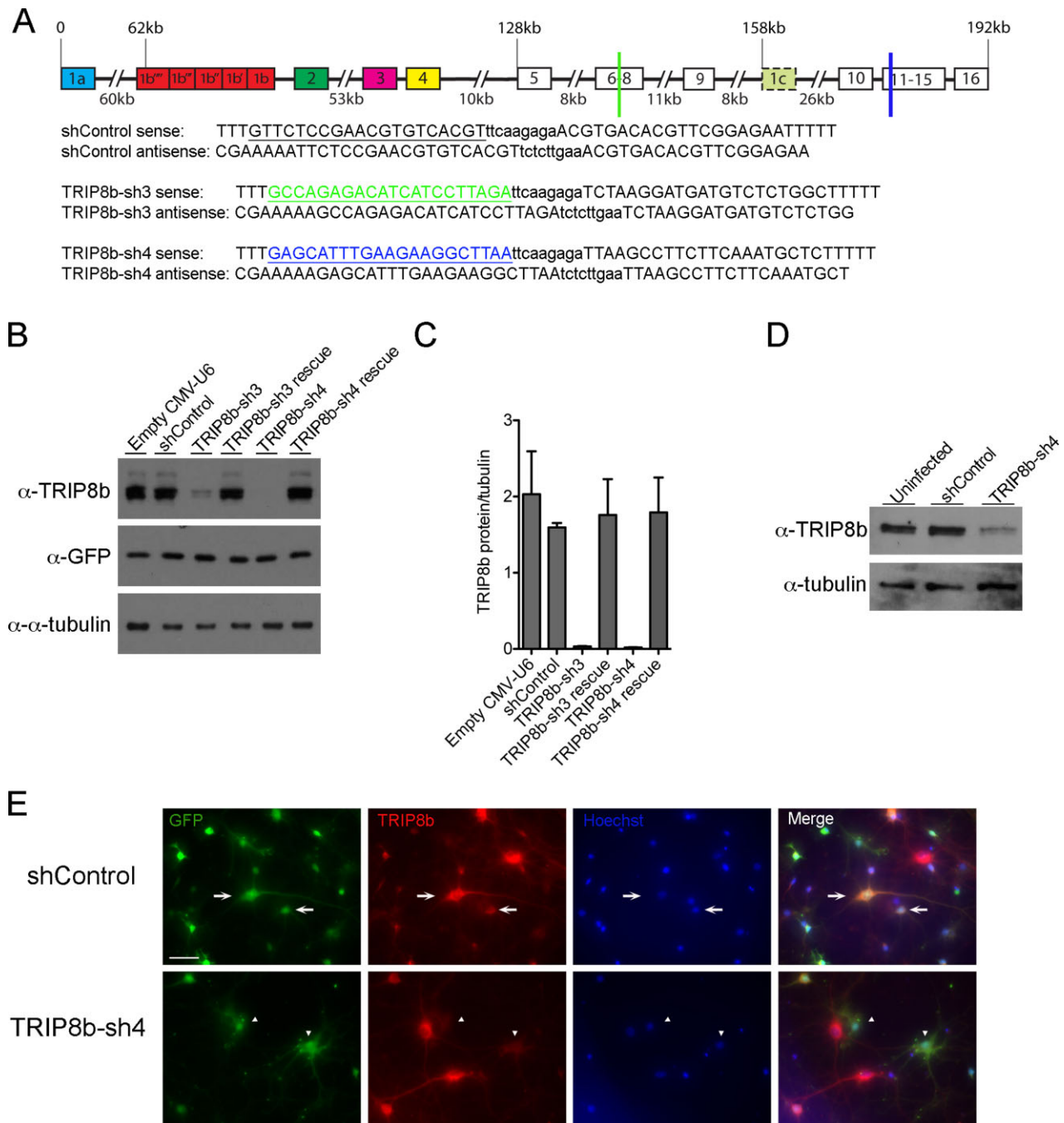

Figure 8. TRIP8b_IsoA4 and IsoA5 are the major isoforms expressed in adult rat hippocampus and whole brain. ***A***, Adult rat hippocampal (Hc, top panel) and whole brain (WB, bottom panel) protein lysates were immunoprecipitated (IP) by TRIP8b exon-specific antibodies, antibody to total TRIP8b, or guinea pig IgG as a control, then probed with antibody to total TRIP8b, demonstrating that the majority of TRIP8b in these two samples does not contain exon 2, implying that IsoA4 and IsoA5 constitute the two major isoforms in hippocampus and whole brain. Input is 10% of total lysate immunoprecipitated. Equal amounts of input and epitope-depleted supernatant (Sup) were loaded. ***A′***, Longer exposure of whole-brain blot shown in ***A***. Note the small amount of exon 2-containing isoforms immunoprecipitated. ***B***, HEK293T cells were transiently transfected with IsoB2 and immunoprecipitation using α-Ex 2, or guinea pig IgG was performed followed by blotting for total TRIP8b. IsoB2 was substantially cleared from the supernatant by immunoprecipitation, further demonstrating exon 2 antibody is effective for immunoprecipitation. Input is 10% of total lysate immunoprecipitated. Equal amounts of input and Sup were loaded. Molecular mass markers are shown in kilodaltons (kD).

cipitated either the lower (presumed IsoA5) or upper (presumed IsoA4) bands, respectively, whereas the alternate band remained in the supernatant (Fig. 8*A*). In summary, we conclude that the most abundant TRIP8b isoforms in brain are IsoA4 and IsoA5, isoforms that upregulate h channel current density and surface expression.

Knockdown of TRIP8b expression in hippocampal neurons downregulates native I_h

Based on isoform abundance correlated with our *in vitro* functional assays, we predicted that most TRIP8b in the brain would promote surface expression of h channels and therefore enhance I_h. If so, then reducing TRIP8b expression with short hairpin RNA (shRNA) should reduce I_h. We first developed effective shRNA constructs, TRIP8b-sh3 and TRIP8b-sh4, which target the *Pex5l* transcript in regions common to all alternatively spliced isoforms (Fig. 9*A*). Coexpression of TRIP8b-sh3 or TRIP8b-sh4

A

shControl sense: TTT<u>GTTCTCCGAACGTGTCACGT</u>ttcaagagaACGTGACACGTTCGGAGAATTTTT
shControl antisense: CGAAAAATTCTCCGAACGTGTCACGTttctcttgaaACGTGACACGTTCGGAGAA

TRIP8b-sh3 sense: TTT<u>GCCAGAGACATCATCCTTAGA</u>ttcaagagaTCTAAGGATGATGTCTCTGGCTTTTT
TRIP8b-sh3 antisense: CGAAAAAGCCAGAGACATCATCCTTAGAtctcttgaaTCTAAGGATGATGTCTCTGG

TRIP8b-sh4 sense: TTT<u>GAGCATTTGAAGAAGGCTTAA</u>ttcaagagaTTAAGCCTTCTTCAAATGCTCTTTTT
TRIP8b-sh4 antisense: CGAAAAAGAGCATTTGAAGAAGGCTTAAtctcttgaaTTAAGCCTTCTTCAAATGCT

B

C

D

E

Figure 9. TRIP8b shRNAs are effective and specific for knockdown of TRIP8b expression in transfected HEK293T cells and cultured hippocampal neurons. **A**, Schematic of *Pex5l* illustrating the site of targeting by TRIP8b-sh3 (light green, exon 6–7 junction) and TRIP8b-sh4 (dark blue, exon 11). Neither shRNA construct targets *Pex5l* in the alternatively spliced region. shControl is not predicted to target any known rat or mouse gene. Sense sequences are underlined. The loop sequence is ttcaagaga. TTTTT is the polymerase III transcription termination sequence. **B**, HEK293T cells were cotransfected with TRIP8b IsoA4 or rescue constructs containing two nucleotide silent mutations in the targeted regions of TRIP8b IsoA4, pCMV-U6 containing either TRIP8b-sh3, TRIP8b-sh4, shControl, or no hairpin, and GFP (to serve as a control for transfection efficiency). After 48 h, cells were lysed, separated by SDS-PAGE, and blotted for TRIP8b, GFP, and α-tubulin, demonstrating that both hairpin constructs are effective for TRIP8b knockdown and are specific for their targeted regions. **C**, Quantitation of TRIP8b knockdown ($n = 3$). **D**, DIV 10 hippocampal neurons were infected with equal titers of FUGWlinker-shControl or FUGWlinker-TRIP8b-sh4 for 11 d, followed by Western blotting for TRIP8b and α-tubulin, confirming that FUGWlinker-TRIP8b-sh4 is effective for knockdown of endogenous TRIP8b in cultured neurons, whereas FUGWlinker-shControl does not alter endogenous TRIP8b compared with uninfected neurons. **E**, DIV 12 hippocampal neurons were infected with FUGWlinker-shControl or TRIP8b-sh4 and 6 d later stained for GFP (green) and TRIP8b (red), as well as for cell nuclei with Hoechst stain (blue). TRIP8b staining remained present in many neurons infected with FUGWlinker-shControl (top panel, arrows), whereas infection with FUGWlinker-TRIP8b-sh4 reduced endogenous TRIP8b staining in many infected neurons (bottom panel, arrowheads). Camera acquisition settings were identical for top and bottom panels. Scale bar: **E**, 50 μm.

with TRIP8b IsoA4 in HEK293T cells demonstrated that both constructs were highly effective at TRIP8b knockdown, whereas shControl, an shRNA construct designed not to target any known rat or mouse gene (Bartkowska et al., 2007) did not alter TRIP8b levels. Furthermore, silent mutation of two nucleotides in the respective shRNA-targeted regions of TRIP8b abolishes knockdown, confirming shRNA specificity (Fig. 9 B,C). We then expressed TRIP8b-sh4 in cultured hippocampal neurons using len-

tivirus, and found decreased expression of endogenous TRIP8b compared with uninfected control cells, whereas viral expression of shControl did not alter levels of endogenous TRIP8b (Fig. 9D). Finally, immunocytochemistry of hippocampal neurons also demonstrated highly efficient infection of cultured neurons and confirmed knockdown of endogenous TRIP8b by lentiviral-expressed TRIP8b-sh4 when compared with uninfected or shControl-infected neurons (Fig. 9E).

Having identified effective and specific shRNA constructs, we then assessed the effects of TRIP8b knockdown on native I_h by whole-cell patch clamp recording of cultured hippocampal neurons (Fig. 10A). Uninfected cells and cells infected with empty virus or TRIP8b shControl were pooled and collectively considered the control group. Maximum I_h amplitude of neurons infected with TRIP8b-sh4 lentivirus (TRIP8b shRNA, shown in red) was significantly reduced compared with control neurons (shown in black) (control: median = 128.55; interquartile range = 29.98, 232.36; $n = 25$; shRNA: median = 35.95; interquartile range = 6.5, 64.76; $n = 15$; $p < 0.005$) (Fig. 10B,C). Note that control cultured hippocampal neurons, consistent with previous data, demonstrate significant variability in current amplitude (Santoro et al., 2004). As expected from a reduction in I_h, TRIP8b shRNA-infected cells also showed significantly decreased voltage sag (control: median = 0.90828, interquartile range = 0.87119, 0.94954; $n = 16$; shRNA: median = 0.99208; interquartile range = 0.96991, 1.0008; $n = 12$; $p < 0.001$) (Fig. 10D). Although TRIP8b exhibited a small but significant hyperpolarizing shift in HCN1-channel gating in heterologous cells, effects of TRIP8b shRNA on gating of h channels were not measured because of the space clamp limitation created by the extensive dendritic arborization of neurons in culture, as well as absent or low currents in many neurons infected with TRIP8b shRNA-expressing lentivirus. Nonetheless, TRIP8b shRNA-infected hippocampal neurons exhibited significantly increased input resistance, suggesting that the dominant function of TRIP8b in hippocampal neurons is to enhance I_h, even at resting membrane potentials (see supplemental Table 2, available at www.jneurosci.org as supplemental material). Together, these data demonstrate that knockdown of endogenous TRIP8b leads to significant downregulation of native I_h, suggesting that the TRIP8b isoforms normally expressed in hippocampal neurons augment h channel function.
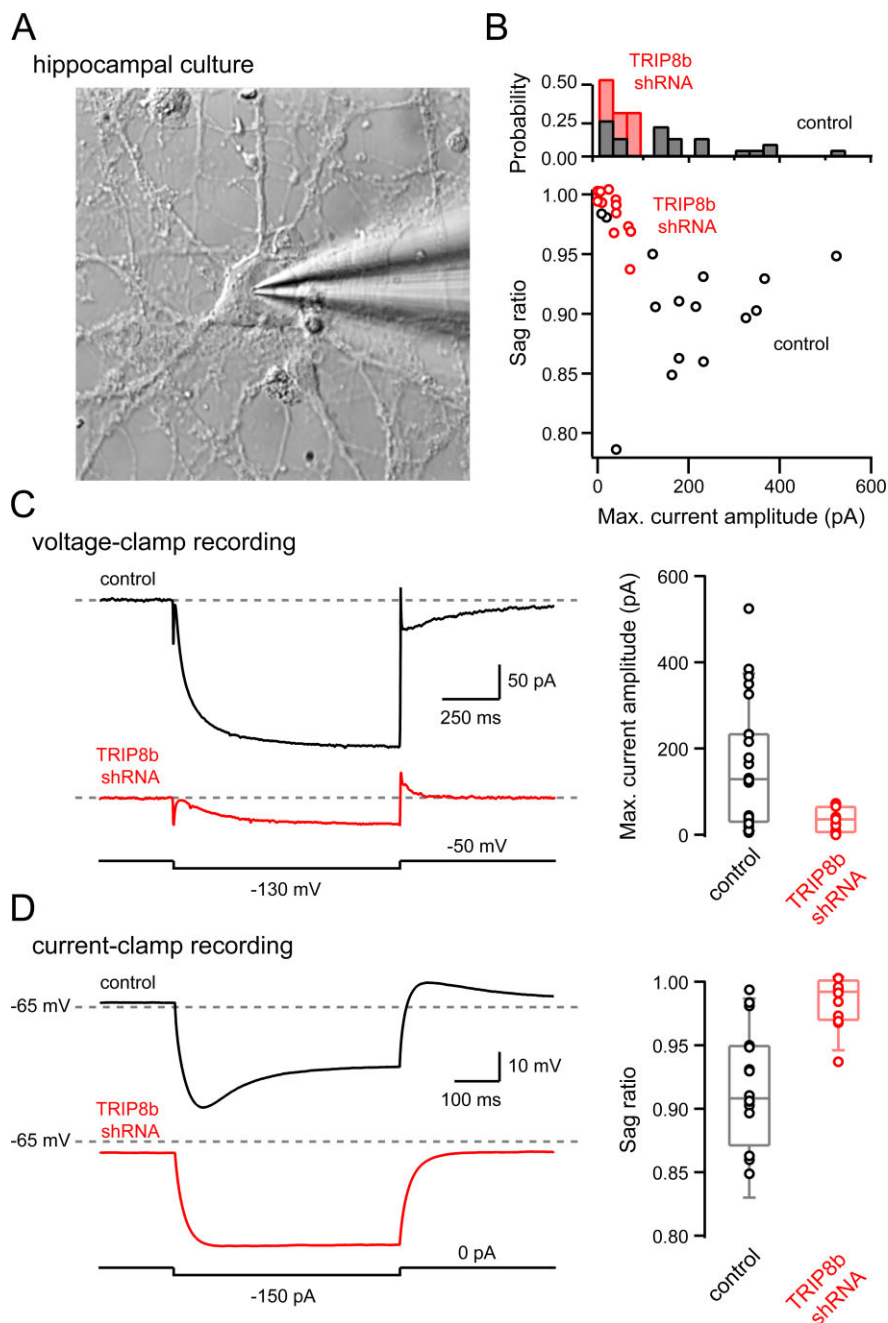
Figure 10. TRIP8b knockdown decreases I_h in cultured hippocampal neurons. **A**, Photomicrograph of a representative recorded hippocampal neuron for these experiments. **B**, Top, Distribution histogram of h-channel current amplitude in control (black, $n = 25$) and shRNA-treated (red, $n = 15$) neurons. Bottom, Voltage sag ratio was displayed as a function of h-channel current amplitude. **C**, Left, Representative, leak-subtracted h-channel current traces of a neuron in control (black) and shRNA-treated (red) cultures recorded under voltage clamp (step to −130 mV from a holding potential of −50 mV). Note the diminished maximal current amplitude after TRIP8b knockdown. Right, Box plots summarizing maximal current amplitude evoked with a voltage step in control (black, $n = 25$) and shRNA-treated (red, $n = 15$) cells. $p < 0.005$, Mann–Whitney U test. **D**, Left, Representative voltage response (to a −150 pA current step) of a neuron in control (black) and shRNA-treated (red) cultures recorded under current-clamp mode. Note the abolition of voltage sag after TRIP8b knockdown. Right, Box plots summarizing voltage sag ratio (calculated as steady-state/trough voltage) evoked with a 500 ms current step in control (black, $n = 16$) and shRNA-treated (red, $n = 12$) cells. $p < 0.001$, Mann–Whitney U test.

Discussion

This study probes the role of the h channel interacting protein TRIP8b in regulating h channel trafficking and function. It shows that the N terminus of TRIP8b is subject to extensive alternative splicing that leads to expression of multiple distinct TRIP8b iso-

forms. Alternatively spliced TRIP8b isoforms differentially up-regulate or downregulate h channel current density, effects largely attributable to control of h channel surface expression. Assessment of the expression of TRIP8b splice variants reveals that the most abundant TRIP8b isoforms upregulate h channel function, suggesting TRIP8b chiefly serves to augment h channel function in brain. Along these lines, we observed that knockdown of TRIP8b in hippocampal neurons dramatically reduced I_h. Overall, our findings are consistent with TRIP8b playing a central role in controlling h channel trafficking and function in the brain, and suggest that expression of a unique TRIP8b isoform or combination of isoforms could determine h channel subcellular localization and function in individual neurons.

Throughout the nervous system, alternative splicing of ion channels (Francesconi and Duvoisin, 2002; Mu et al., 2003; Jaskolski et al., 2004) and ion channel binding or scaffolding proteins (Chetkovich et al., 2002; DeSouza et al., 2002) allows exquisite and diverse control of ion channel trafficking and function. Invertebrate h channels are extensively alternatively spliced (Gisselmann et al., 2004; Ouyang et al., 2007), but the most abundant h channel subunits of the vertebrate brain, HCN1, HCN2, and HCN4, are not known to undergo alternative splicing. Our finding that an h channel auxiliary subunit exhibits extensive and functionally important alternative splicing raises the possibility that TRIP8b splicing might contribute to the marked regional and subcellular variability in the localization and function of h channels throughout the brain (Santoro and Baram, 2003; Notomi and Shigemoto, 2004).

Our discovery and characterization of multiple TRIP8b isoforms is helpful for reconciling previous studies on TRIP8b. Chen et al. (2001b) originally reported that TRIP8b (IsoA4) interacted with Rab8b and had a stimulatory effect on cAMP-induced secretion of ACTH in AtT20 cells, suggesting a role for this isoform in the forward trafficking of vesicles to surface membrane. However, Santoro et al. (2004) found that overexpression of a different isoform of TRIP8b (IsoB2) with HCN subunits in oocytes and HEK293 cells decreased HCN protein surface expression and I_h, and that overexpression of IsoB2 in hippocampal neurons reduced native I_h. Downregulation of I_h by TRIP8b was unexpected in light of the earlier study and the observation that TRIP8b was enriched in distal dendrites where I_h is maximal. Our data help explain these seemingly disparate results. Whereas the IsoB2 studied by Santoro et al. (2004) downregulates I_h and h channel subunit surface expression, we show that it is not abundant in hippocampus. Along these lines, the fact that knockdown of endogenous TRIP8b in hippocampal pyramidal neurons reduces I_h suggests that one or more of the surface expression-enhancing TRIP8b isoforms (rather than IsoB2) control h channel function in individual pyramidal neurons. We thus conclude that the role of endogenous TRIP8b in hippocampal pyramidal neurons is to augment I_h, which is expected to dampen passive signal propagation and reduce temporal summation of synaptic signals originating in distal dendrites (Magee, 1998, 1999), as well as to constrain synaptic plasticity (Nolan et al., 2004) and Ca^{2+}-channel signaling in distal dendrites (Tsay et al., 2007). Predicting the functional effects of TRIP8b in other neurons depends on the role of I_h in those neurons and which TRIP8b isoform or set of isoforms is expressed. Although based on isoform abundance TRIP8b is predicted to enhance I_h in most neurons, it is possible that a rare TRIP8b isoforms such as IsoB2 might dominantly inhibit h channel trafficking and function in distinct neurons.

Because we find that different TRIP8b isoforms exhibit distinct effects on h channel surface expression, we reason that dif-ferentially included exons of alternatively spliced TRIP8b isoforms may contain sorting signals that specify the subcellular routing of TRIP8b and its h channel binding partner. Alternative exon-encoded domains could facilitate trafficking to plasma membrane [similar to the T1 domain in Kv1 channels (Rivera et al., 2005)], or promote endocytosis [such as the dileucine motif in Na1.2 channels (Garrido et al., 2001)]. Along these lines, TRIP8b exon 4 contains a consensus dileucine sequence (DEXXXL[LI]) (Bonifacino and Traub, 2003) that could promote clathrin-dependent endocytosis of exon 4-containing isoforms. However, we did not observe downregulation of h channels by any of the exon 4-containing isoforms [indeed, comparing TRIP8b isoforms that differed only by the presence of exon 4 (IsoA4 vs IsoA5 and IsoB1 vs IsoB2) revealed that currents elicited by exon 4-containing isoforms were significantly larger]. Exon 2 contains a tyrosine based consensus sequence (YXXϕ) that could also promote endocytosis via distinct adapter protein complexes. Although exon 2-containing IsoB2 indeed downregulated h channel surface expression, this downregulation appeared independent of exon 2, as the exon 2-containing IsoB1, IsoB3, and IsoB4 all enhanced HCN1 current. Because these data were obtained in overexpression studies in heterologous cells, further experiments are certainly required to characterize the complete mechanisms by which different exons influence trafficking and targeting of h channels within neurons.

The gene encoding TRIP8b (*Pex5l*) is derived from ancestral duplication of the gene encoding the peroxisomal import receptor, peroxin 5 (*Pex5*), and structural homology between the two proteins predicts the molecular interactions of TRIP8b (Gatto et al., 2000; Stanley and Wilmanns, 2006). Cargo binding to peroxin 5 exposes N-terminal regions for targeting and delivery of cargo to peroxisomes (Holroyd and Erdmann, 2001; Gouveia et al., 2003). By homology, we reason that interaction with HCN subunits (via the TRIP8b C terminus) could expose alternatively spliced N-terminal TRIP8b protein domains that mediate different trafficking functions. Consistent with a requirement for HCN subunit interaction for proper trafficking, we found TRIP8b isoforms overexpressed in neurons are trafficked to different subcellular locations depending on whether they are coexpressed with HCN1. Further suggesting a role for cargo binding in trafficking, TRIP8b enrichment in distal dendrites of cortical but not hippocampal pyramidal neurons is disrupted in the HCN1 knock-out mouse (Santoro et al., 2004). Hippocampal pyramidal neurons (as opposed to cortical pyramidal neurons) express high levels of HCN2. Thus in the HCN1 knock-out mouse, TRIP8b might be coenriched with HCN2 in distal dendrites of hippocampal pyramidal neurons, but the lack of sufficient quantities of an HCN subunit prevents TRIP8b dendritic targeting in cortical pyramidal neurons.

Although unique isoforms differentially influenced h channel trafficking, all TRIP8b isoforms had similar effects on h channel gating, causing a hyperpolarizing shift in voltage dependence of channel activation. In addition to the previously published interaction between TRIP8b and the h channel extreme C terminus (Santoro et al., 2004), we also found that the TRIP8b C terminus common to all splice variants mediated interaction with the HCN1 CNBD. Because of the importance of the CNBD in h channel gating (Wainger et al., 2001; Wang et al., 2001), we reason that the TRIP8b interaction with the HCN1 CNBD could introduce steric effects to alter h channel gating. Because the CNBD of different HCN subunits differentially affects gating, it will be important to explore whether TRIP8b similarly alters gating of other homomeric or heteromeric combinations of HCN

subunits. It will also be interesting to determine whether cyclic nucleotides affect the TRIP8b effects on gating of I_h.

Although we find that the h channel-upregulating IsoA4 and IsoA5 are the most abundant isoforms in the brain, mRNA assays show that all TRIP8b isoforms are expressed. It is possible that under some physiological or pathological conditions the relative expression of TRIP8b isoforms might vary, thereby changing the localization and function of h channels. In light of this possibility, it will be important to examine whether TRIP8b alternative splicing plays a role in regulating forms of intrinsic neuronal plasticity dependent on or mediated by h channels (Fan et al., 2005; Brager and Johnston, 2007). Furthermore, because acquired abnormalities of h channel function might underlie the increased seizure propensity in models of temporal lobe epilepsy (Shah et al., 2004; Jung et al., 2007; Shin et al., 2008), TRIP8b splicing should be explored in hippocampal epileptogenesis. Interestingly, we found that in a rat model of temporal lobe epilepsy, HCN1 was downregulated from distal dendrites and mislocalized to subcellular compartments in the soma of hippocampal pyramidal neurons (Shin et al., 2008). This reduction of functional h channels in epileptic animals was associated with reduced interaction between HCN1 and TRIP8b (Shin et al., 2008). Although TRIP8b alternative splicing found in the normal brain does not directly involve the C-terminal domains that mediate h channel subunit interaction, it is possible that disease states such as epilepsy promote yet unknown TRIP8b splicing that reduces the ability of this molecule to bind to and augment h channel function. Future studies to explore the role of TRIP8b in physiological and pathological processes should shed further light on h channel trafficking and may lead to new insights and treatments that benefit patients affected by epilepsy.

References

Amery L, Sano H, Mannaerts GP, Snider J, Van Looy J, Fransen M, Van Veldhoven PP (2001) Identification of PEX5p-related novel peroxisome-targeting signal 1 (PTS1)-binding proteins in mammals. Biochem J 357:635–646.

Bartkowska K, Paquin A, Gauthier AS, Kaplan DR, Miller FD (2007) Trk signaling regulates neural precursor cell proliferation and differentiation during cortical development. Development 134:4369–4380.

Beck H, Yaari Y (2008) Plasticity of intrinsic neuronal properties in CNS disorders. Nat Rev Neurosci 9:357–369.

Bonifacino JS, Traub LM (2003) Signals for sorting of transmembrane proteins to endosomes and lysosomes. Annu Rev Biochem 72:395–447.

Brager DH, Johnston D (2007) Plasticity of intrinsic excitability during long-term depression is mediated through mGluR-dependent changes in I_h in hippocampal CA1 pyramidal neurons. J Neurosci 27:13926–13937.

Brewster A, Bender RA, Chen Y, Dube C, Eghbal-Ahmadi M, Baram TZ (2002) Developmental febrile seizures modulate hippocampal gene expression of hyperpolarization-activated channels in an isoform- and cell-specific manner. J Neurosci 22:4591–4599.

Chen K, Aradi I, Thon N, Eghbal-Ahmadi M, Baram TZ, Soltesz I (2001) Persistently modified h-channels after complex febrile seizures convert the seizure-induced enhancement of inhibition to hyperexcitability. Nat Med 7:331–337.

Chen S, Wang J, Siegelbaum SA (2001a) Properties of hyperpolarization-activated pacemaker current defined by coassembly of HCN1 and HCN2 subunits and basal modulation by cyclic nucleotide. J Gen Physiol 117:491–504.

Chen S, Liang MC, Chia JN, Ngsee JK, Ting AE (2001b) Rab8b and its interacting partner TRIP8b are involved in regulated secretion in AtT20 cells. J Biol Chem 276:13209–13216.

Chen X, Sirois JE, Lei Q, Talley EM, Lynch C 3rd, Bayliss DA (2005) HCN subunit-specific and cAMP-modulated effects of anesthetics on neuronal pacemaker currents. J Neurosci 25:5803–5814.

Chetkovich DM, Bunn RC, Kuo SH, Kawasaki Y, Kohwi M, Bredt DS (2002) Postsynaptic targeting of alternative postsynaptic density-95 isoforms by distinct mechanisms. J Neurosci 22:6415–6425.

Chung WK, Shin M, Jaramillo TC, Leibel RL, LeDuc CA, Fischer SG, Tzilianos E, Gheith AA, Lewis AS, Chetkovich DM (2009) Absence epilepsy in apathetic, a spontaneous mutant mouse lacking the h channel subunit, HCN2. Neurobiol Dis 33:499–508.

Cuadra AE, Kuo SH, Kawasaki Y, Bredt DS, Chetkovich DM (2004) AMPA receptor synaptic targeting regulated by stargazin interactions with the Golgi-resident PDZ protein nPIST. J Neurosci 24:7491–7502.

D'Andrea LD, Regan L (2003) TPR proteins: the versatile helix. Trends Biochem Sci 28:655–662.

DeSouza S, Fu J, States BA, Ziff EB (2002) Differential palmitoylation directs the AMPA receptor-binding protein ABP to spines or to intracellular clusters. J Neurosci 22:3493–3503.

Dittgen T, Nimmerjahn A, Komai S, Licznerski P, Waters J, Margrie TW, Helmchen F, Denk W, Brecht M, Osten P (2004) Lentivirus-based genetic manipulations of cortical neurons and their optical and electrophysiological monitoring in vivo. Proc Natl Acad Sci U S A 101:18206–18211.

Fan Y, Fricker D, Brager DH, Chen X, Lu HC, Chitwood RA, Johnston D (2005) Activity-dependent decrease of excitability in rat hippocampal neurons through increases in I(h). Nat Neurosci 8:1542–1551.

Francesconi A, Duvoisin RM (2002) Alternative splicing unmasks dendritic and axonal targeting signals in metabotropic glutamate receptor 1. J Neurosci 22:2196–2205.

Garrido JJ, Fernandes F, Giraud P, Mouret I, Pasqualini E, Fache MP, Jullien F, Dargent B (2001) Identification of an axonal determinant in the C-terminus of the sodium channel Na(v) 1.2. EMBO J 20:5950–5961.

Gatto GJ Jr, Geisbrecht BV, Gould SJ, Berg JM (2000) A proposed model for the PEX5-peroxisomal targeting signal-1 recognition complex. Proteins 38:241–246.

Gisselmann G, Wetzel CH, Warnstedt M, Hatt H (2004) Functional characterization of Ih-channel splice variants from Apis mellifera. FEBS Lett 575:99–104.

Gouveia AM, Guimarães CP, Oliveira ME, Sá-Miranda C, Azevedo JE (2003) Insertion of Pex5p into the peroxisomal membrane is cargo protein-dependent. J Biol Chem 278:4389–4392.

Holroyd C, Erdmann R (2001) Protein translocation machineries of peroxisomes. FEBS Lett 501:6–10.

Jaskolski F, Coussen F, Nagarajan N, Normand E, Rosenmund C, Mulle C (2004) Subunit composition and alternative splicing regulate membrane delivery of kainate receptors. J Neurosci 24:2506–2515.

Jung S, Jones TD, Lugo JN Jr, Sheerin AH, Miller JW, D'Ambrosio R, Anderson AE, Poolos NP (2007) Progressive dendritic HCN channelopathy during epileptogenesis in the rat pilocarpine model of epilepsy. J Neurosci 27:13012–13021.

Lai HC, Jan LY (2006) The distribution and targeting of neuronal voltage-gated ion channels. Nat Rev Neurosci 7:548–562.

Lo WY, Botzolakis EJ, Tang X, Macdonald RL (2008) A conserved Cys-loop receptor aspartate residue in the M3–M4 cytoplasmic loop is required for GABAA receptor assembly. J Biol Chem 283:29740–29752.

Lois C, Hong EJ, Pease S, Brown EJ, Baltimore D (2002) Germline transmission and tissue-specific expression of transgenes delivered by lentiviral vectors. Science 295:868–872.

Lörincz A, Notomi T, Tamás G, Shigemoto R, Nusser Z (2002) Polarized and compartment-dependent distribution of HCN1 in pyramidal cell dendrites. Nat Neurosci 5:1185–1193.

Ludwig A, Budde T, Stieber J, Moosmang S, Wahl C, Holthoff K, Langebartels A, Wotjak C, Munsch T, Zong X, Feil S, Feil R, Lancel M, Chien KR, Konnerth A, Pape HC, Biel M, Hofmann F (2003) Absence epilepsy and sinus dysrhythmia in mice lacking the pacemaker channel HCN2. EMBO J 22:216–224.

Magee JC (1998) Dendritic hyperpolarization-activated currents modify the integrative properties of hippocampal CA1 pyramidal neurons. J Neurosci 18:7613–7624.

Magee JC (1999) Dendritic Ih normalizes temporal summation in hippocampal CA1 neurons. Nat Neurosci 2:508–514.

Mu Y, Otsuka T, Horton AC, Scott DB, Ehlers MD (2003) Activity-dependent mRNA splicing controls ER export and synaptic delivery of NMDA receptors. Neuron 40:581–594.

Much B, Wahl-Schott C, Zong X, Schneider A, Baumann L, Moosmang S, Ludwig A, Biel M (2003) Role of subunit heteromerization and N-linked glycosylation in the formation of functional hyperpolarization-activated cyclic nucleotide-gated channels. J Biol Chem 278:43781–43786.

Nolan MF, Malleret G, Dudman JT, Buhl DL, Santoro B, Gibbs E, Vronskaya S, Buzsáki G, Siegelbaum SA, Kandel ER, Morozov A (2004) A behavioral role for dendritic integration: HCN1 channels constrain spatial memory and plasticity at inputs to distal dendrites of CA1 pyramidal neurons. Cell 119:719 –732.

Notomi T, Shigemoto R (2004) Immunohistochemical localization of Ih channel subunits, HCN1– 4, in the rat brain. J Comp Neurol 471:241–276.

Ouyang Q, Goeritz M, Harris-Warrick RM (2007) Panulirus interruptus Ih-channel gene PIIH: modification of channel properties by alternative splicing and role in rhythmic activity. J Neurophysiol 97:3880 –3892.

Rivera JF, Chu PJ, Arnold DB (2005) The T1 domain of Kv1.3 mediates intracellular targeting to axons. Eur J Neurosci 22:1853–1862.

Santoro B, Baram TZ (2003) The multiple personalities of h-channels. Trends Neurosci 26:550 –554.

Santoro B, Wainger BJ, Siegelbaum SA (2004) Regulation of HCN channel surface expression by a novel C-terminal protein-protein interaction. J Neurosci 24:10750 –10762.

Shah MM, Anderson AE, Leung V, Lin X, Johnston D (2004) Seizure-induced plasticity of h channels in entorhinal cortical layer III pyramidal neurons. Neuron 44:495–508.

Shin M, Chetkovich DM (2007) Activity-dependent regulation of h channel distribution in hippocampal CA1 pyramidal neurons. J Biol Chem 282:33168 –33180.

Shin M, Simkin D, Suyeoka GM, Chetkovich DM (2006) Evaluation of HCN2 abnormalities as a cause of juvenile audiogenic seizures in Black Swiss mice. Brain Res 1083:14 –20.

Shin M, Brager D, Jaramillo TC, Johnston D, Chetkovich DM (2008) Mis-localization of h channel subunits underlies h channelopathy in temporal lobe epilepsy. Neurobiol Dis 32:26 –36.

Stanley WA, Wilmanns M (2006) Dynamic architecture of the peroxisomal import receptor Pex5p. Biochim Biophys Acta 1763:1592–1598.

Tiscornia G, Singer O, Verma IM (2006) Design and cloning of lentiviral vectors expressing small interfering RNAs. Nat Protoc 1:234 –240.

Tsay D, Dudman JT, Siegelbaum SA (2007) HCN1 channels constrain synaptically evoked Ca2+ spikes in distal dendrites of CA1 pyramidal neurons. Neuron 56:1076 –1089.

Vandenberghe W, Nicoll RA, Bredt DS (2005) Stargazin is an AMPA receptor auxiliary subunit. Proc Natl Acad Sci U S A 102:485– 490.

Wainger BJ, DeGennaro M, Santoro B, Siegelbaum SA, Tibbs GR (2001) Molecular mechanism of cAMP modulation of HCN pacemaker channels. Nature 411:805– 810.

Wang J, Chen S, Siegelbaum SA (2001) Regulation of hyperpolarization-activated HCN channel gating and cAMP modulation due to interactions of COOH terminus and core transmembrane regions. J Gen Physiol 118:237–250.

Williams SR, Stuart GJ (2000) Site independence of EPSP time course is mediated by dendritic I(h) in neocortical pyramidal neurons. J Neurophysiol 83:3177–3182.

Ying SW, Jia F, Abbas SY, Hofmann F, Ludwig A, Goldstein PA (2007) Dendritic HCN2 channels constrain glutamate-driven excitability in reticular thalamic neurons. J Neurosci 27:8719 – 8732.

Zha Q, Brewster AL, Richichi C, Bender RA, Baram TZ (2008) Activity-dependent heteromerization of the hyperpolarization-activated, cyclic-nucleotide gated (HCN) channels: role of N-linked glycosylation. J Neurochem 105:68 –77.